Fine scale modeling of wintertime aerosol mass, number, and size distributions in central California

Yang Zhang,[1] Ping Liu,[1] Xiao-Huan Liu,[1,3] Betty Pun,[2,4] Christian Seigneur,[2,5] Mark Z. Jacobson,[6] and Wen-Xing Wang[3]

Received 3 August 2009; revised 23 October 2009; accepted 12 February 2010; published 12 August 2010.

[1] In light of nonattainment of $PM_{2.5}$ in central California, the CMAQ-MADRID 1 model is applied to simulate $PM_{2.5}$ mass, number, and size distributions observed during the California Regional $PM_{10}/PM_{2.5}$ Air Quality Study (CRPAQS) winter episode of 25–31 December 2000. The simulations with 12 and 24 size sections at a horizontal grid resolution of 4 km reproduce well the 24 h average mass concentrations of $PM_{2.5}$ (with normalized mean biases (NMBs) of −6.2% to 0.5%), but with larger biases for organic matter, nitrate, and elemental carbon (with NMBs of −67% to 40.2%) and a weaker capability of replicating temporal variation of $PM_{2.5}$ and its components. The coagulation process leads to a 40%–91% reduction in simulated $PM_{2.5}$ number concentrations. The 24 section simulation with coagulation shows the best agreement with the observed PM number and size distributions (with an NMB of −13.9%), indicating the importance of coagulation for predicting particle number and the merits of using a fine particle size resolution. Accurately simulating $PM_{2.5}$ number and size distributions continue to be a major challenge, due to inaccuracies in model inputs (e.g., meteorological fields, precursor emissions, and the initial size distribution of PM emissions and concentrations), uncertainties in model formulations (e.g., heterogeneous chemistry and aerosol formation, growth, and removal processes), as well as inconsistencies and uncertainties in observations obtained with different methods.

Citation: Zhang, Y., P. Liu, X.-H. Liu, B. Pun, C. Seigneur, M. Z. Jacobson, and W.-X. Wang (2010), Fine scale modeling of wintertime aerosol mass, number, and size distributions in central California, *J. Geophys. Res.*, *115*, D15207, doi:10.1029/2009JD012950.

1. Introduction

[2] With more stringent National Ambient Air Quality Standards (NAAQSs) set by the U.S. Environmental Protection Agency (U.S. EPA) (35 μg m^{-3} for the 24 h average fine particulate matters with an aerodynamic diameter less than or equal to 2.5 μm ($PM_{2.5}$), effective on 17 December 2006, and 0.075 ppm for the 8 h ozone (O_3), effective on 27 May 2008; http://www.epa.gov/air/criteria.html), central California (CA) continues to be one of the nonattainment areas with the highest max 8 h O_3 and $PM_{2.5}$ concentrations in the United States. During the winter, the Great Basin high-pressure system often stays over this region for several days to weeks, resulting in a strong large scale subsidence temperature inversion that forms a lid over the air basin and confines pollutants within the planetary boundary layer (PBL) [*Watson et al.*, 1998]. At night, radiation inversions often occur as near surface air parcels cool radiatively, trapping pollutants in the nocturnal PBL with a shallow mixing depth and low ventilation rate. The combined large scale subsidence and radiation inversions, coupled with large area sources (e.g., cooking, residential wood combustion), mobile sources (e.g., diesel, gasoline), and agricultural sources (e.g., livestock and soil), lead to high PM concentrations, particularly over the San Joaquin Valley (SJV) [*Chow et al.*, 1993, 2006; *Herner et al.*, 2005; *Ying and Kleeman*, 2006; *Ying et al.*, 2008a]. High $PM_{2.5}$ levels often occur during winter and can contribute to 50%–75% of annual average concentrations [*Chow et al.*, 1993, 2006]. Among all $PM_{2.5}$ species, ammonium nitrate (NH_4NO_3) can contribute to 30%–60% of $PM_{2.5}$ during winter [*Magliano et al.*, 1999; *Chow et al.*, 1999; *Watson and Chow*, 2002; *Herner et al.*, 2005; *Ying and Kleeman*, 2006]. The peak concentrations of ultrafine PM with an aerodynamic diameter less than or equal to 0.1 μm, $PM_{0.1}$, in central CA are among the highest in the United States [*Herner et al.*, 2005], which contribute to the

[1]Department of Marine, Earth, and Atmospheric Sciences, North Carolina State University, Raleigh, North Carolina, USA.
[2]Atmospheric and Environmental Research, Inc., San Ramon, California, USA.
[3]Environment Research Institute, Shandong University, Jinan City, Shandong Province, China.
[4]Calera Corporation, Los Gatos, California, USA.
[5]Cerea, Joint Laboratory École des Ponts Paris Tech/EDF R&D, Université Paris-Est, Champs sur-Marne, France.
[6]Department of Civil and Environmental Engineering, Stanford University, Stanford, California, USA.

Copyright 2010 by the American Geophysical Union.
0148-0227/10/2009JD012950

mass concentrations of larger particles through various growth processes (e.g., heterogeneous nucleation, coagulation, condensation) and may be of particular public health concerns [*Oberdörster*, 1996; *Ibald-Mulli et al.*, 2002; *Becker et al.*, 2003]. The observed PM_{10} number concentrations and number mean diameters range from 2700 to 89,000 cm^{-3} and 0.021 to 0.109 μm, with an average of 22,000 cm^{-3} and 0.066 μm, respectively [*Watson et al.*, 2002]. Understanding the mass, number, size distribution, and formation mechanism of $PM_{2.5}$ is therefore crucial to the development of effective emission control strategies for $PM_{2.5}$ attainment and climate mitigation in this region. The California Regional $PM_{10}/PM_{2.5}$ Air Quality Study (CRPAQS), a 14 month (December 1999 to February 2001) long intensive field program launched by the California Air Resources Board (CARB) and conducted over the SJV and surrounding air basins (i.e., Sacramento Valley and San Francisco Bay) by multiple collaborative organizations, was designed to improve the understanding of the causes of high PM levels in central CA in order to develop cost-effective control strategies [*Watson et al.*, 1998].

[3] Compared with the Los Angeles Basin where extensive modeling studies have been conducted [e.g., *Harley et al.*, 1993, 1997; *Jacobson*, 1997; *Lurmann et al.*, 1997; *Zhang et al.*, 2004; *Jacobson et al.*, 2007], fewer 3-D model simulations have been conducted for the northern and central CA, e.g., those focusing on O_3 include 3–6 August 1990 by *DaMassa et al.* [1996], *Lu and Chang* [1998], *Dabdub et al.* [1999], and *Jacobson* [2001]; 25–31 July 2000 by *Tonse et al.* [2008]; and 29 July to 3 August 2000 by *Jin et al.* [2008]; those focusing on $PM_{2.5}$ include 4–6 January 1996 by *Held et al.* [2004], *Kleeman et al.* [2005], and *Ying and Kleeman* [2006]; 25–31 December 2000 by *Pun et al.* [2009]; 25 December 2000 to 7 January 2001 by *Liang et al.* [2006] and *Ying et al.* [2008a, 2008b]; and 17 December 2000 to 7 January 2001 by *Livingstone et al.* [2009]. Most of these PM modeling studies used coarse-to-medium size resolutions with 3 P.M. modes or 2–15 size sections between 0.01 and 10 μm and focused on the simulation of PM mass concentrations (e.g., some neglected homogeneous nucleation, see *Ying et al.* [2008b]). In this study, the Community Multiscale Air Quality Modeling system with the Model of Aerosol Dynamics, Reaction, Ionization, and Dissolution (CMAQ-MADRID 1) [*Zhang et al.*, 2004; *Pun et al.*, 2006] is applied to central and northern California to simulate air pollutants for the period of 25–31 December 2000 during the CRPAQS. Compared with previous studies for the same CRPAQS episode [*Liang et al.*, 2006; *Pun et al.*, 2009; *Ying et al.*, 2008], this study presents a comprehensive evaluation of gases and PM species mass concentrations and PM number and size distributions using nearly all measurements available from CARB at all sites. None of the previous studies evaluated simulated particle size distribution and number concentrations from 3-D air quality models, which is the focus of the model evaluation in this paper. While *Pun et al.* [2009] used CMAQ and CMAQ-MADRID 1 with two PM size sections, this study uses high PM size resolutions of 12 and 24 size sections between 0.001 and 10 μm to assess the model's capability in reproducing mass concentration, number concentration, and size distribution of $PM_{2.5}$. The objectives of this study are to evaluate CMAQ-MADRID's capability of simulating PM mass and number concentrations as well as size distributions in the central CA and to understand the formation mechanism underlying the high PM concentrations to support $PM_{2.5}$ attainment effort in this area. Evaluating PM number concentrations and size distributions has important climatic implications, as they directly affect simulated cloud droplet number concentrations and radiative budget via indirect effects of aerosols.

2. Episode and Model Description

[4] The episode simulated is 25–31 December 2000, which is the first week of a 2 week episode (25 December 2000 and 7 January 2001) selected by CARB for meteorological modeling. During the 2 week episode, strong high-pressure aloft along the West Coast created subsidence and stable weather over the region, with an accompanying strong surface high located over Idaho. With high pressure over the intermountain region and lower pressures over the eastern Pacific, moderate offshore flow developed. The normal nocturnal inversion at the surface was then reinforced with a subsidence inversion aloft, created by adiabatic warming off the Sierra's and general subsidence from the ridge. As the West Coast ridge was building into CA, PBL mixing heights became lower and stability increased, limiting afternoon mixing and resulting in the maximum PM measurements of the CRPAQS winter study period [*Ferreria and Shipp*, 2005]. The peak PM_{10} concentration of 208 $\mu g\ m^{-3}$ was recorded at Fresno on 4 January, and the peak $PM_{2.5}$ concentration of 179 $\mu g\ m^{-3}$ was recorded at Edison in the Southern Valley near Bakersfield on 1 January [*Turkiewicz et al.*, 2006]. The combination of weak offshore flow and midtropospheric stability caused elevated PM concentrations (e.g., $PM_{2.5}$ concentrations of 131–179 $\mu g\ m^{-3}$) across central CA. The meteorological fields for this 2 week episode were provided by CARB. They were generated using the fifth generation PSU/National Center for Atmospheric Research (NCAR) Mesoscale Model (MM5) version 3.6.3 and processed into CMAQ-ready format using Meteorology-Chemistry Interface Processor (MCIP) 3.1. MM5 tends to overpredict temperatures by about 2 K at surface and nighttime and wind speed by 0.73 $m\ s^{-1}$ on average [*Pun et al.*, 2009]. MM5 reproduces observed meteorological conditions reasonably well although the quality of the meteorological simulation deteriorated after 31 December (California Air Resources Board, personal communication, *Kaduwela*, 2006; *Kemal Gurer*, 2009) [*Livingstone et al.*, 2009], limiting the use of those meteorological fields to the first half of the episode between 25 and 31 December 2000 for air quality simulations in this study [*Pun et al.*, 2009].

[5] The air quality model used is CMAQ-MADRID 1. The version used here is based on CMAQ version 4.6 [*Byun and Schere*, 2006] and the aerosol module of MADRID 1 of *Zhang et al.* [2004] with updates from the study of *Pun et al.* [2005] and this study. CMAQ v4.6 offers a number of options for diffusion and advection schemes and gas-phase chemical mechanisms. In this study, the asymmetric convective model version 2 (ACM2) and the multiscale algorithm are used for vertical and horizontal diffusion, respectively. The mass-conserving Yamartino scheme is used for horizontal and vertical advection. The cloud module is based on the ACM algorithm. The gas-phase and aqueous-phase chemical mechanisms are based on the Statewide Air Pollution

Research Center (SAPRC) mechanism and the Regional Acid Deposition Model (RADM) mechanism, respectively. Compared with MADRID 1 of *Zhang et al.* [2004], several major modifications have been made in the updated MADRID 1 version used in this study. First, the number of surrogates of secondary organic aerosol (SOA) compounds has been reduced from 38 (4 anthropogenic and 34 biogenic) to 25 (7 anthropogenic and 18 biogenic) to simulate SOA more efficiently. SOA formation from the oxidation of isoprene, monoterpenes, and sesquiterpene is accounted for. Second, MADRID 1 has been coupled with SAPRC99, allowing the use of a more detailed gas-phase mechanism for volatile organic compounds (VOCs) than the Carbon Bond Mechanism version IV (CBM-IV) and the Regional Acid Deposition Mechanism version 2 (RADM2). Third, the coagulation algorithm of *Jacobson et al.* [1994] has been incorporated into MADRID 1 to provide a more realistic representation of $PM_{2.5}$ number concentrations and size distribution. This code conserves total particle volume and volume concentration, as coagulation physically does, is positive-definite, noniterative, and stable. As described by *Zhang et al.* [2004], the moving-center technique of *Jacobson* [1997] is used in MADRID to simulate the growth of particles due to various growth processes (e.g., coagulation, condensation, and aqueous-phase chemistry). As all 3-D sectional aerosol models, this technique uses fixed size boundaries and allows particle movement within and across the boundaries. However, the representative size of a given particle size section is not fixed, which allows one to solve jointly for the mass and number concentrations (models that use a fixed diameter for each size section solve the general dynamic equation for only one variable; if it solves for the mass concentration, the number concentration that would be estimated from the mass concentration and section representative diameter would be incorrect, and a separate solution must be obtained for the number concentration). Finally, the number of particle size section has been increased from 2 to 8 to 12 and 24 for PM_{10} size representation between 0.001 to 10 μm at a finer resolution. As a result of these changes, the updated MADRID 1 in this study explicitly simulates 112 gaseous species and 40 aerosol species and 1 aerosol number in 12 and 24 sections (a total of 492 and 984 prognostic variables for aerosol mass and number concentrations).

[6] CMAQ-MADRID 1 simulations with 12 and 24 size sections (referred to as the 12 sec and the 24 sec simulations hereafter) are conducted at a 4 km horizontal grid spacing (185 × 185 horizontal grid cells) over a domain that covers central and northern CA, including the entire SJV and a portion of Nevada, as shown in Figure 1. The vertical resolution includes 15 layers from the surface to the tropopause, with the first layer heights of 25.8–30.5 m. The 4 km resolution emissions of gases and PM species are also based on CMAQ-ready emissions provided by CARB. Gridded emissions were compiled by CARB and the University of California at Davis (UCD) based on point, area, mobile, and natural sources. Chemical emission profiles and corresponding diurnal variations are from an in-house library at CARB. Those for elemental carbon (EC) and organic carbon (OC) are based on the National Institute for Occupational Safety and Health (NIOSH) method [*Held et al.*, 2004; *Ying et al.*, 2008b]. More detailed information on CARB emission inventories can be found at http://www.arb.ca.gov/ei/ei.htm. The CARB CMAQ-ready emissions in Aitken and accumulation modes are mapped into the sectional representations using the CMAQ-MADRID preprocessor in which the size-resolved mass-weighting factors are derived by integrating the lognormal function for respective size sections, namely, the emissions of Aitken and accumulation modes are mapped into sections 1–10 and 1–20 for the 12- and 24 section representations, respectively, and those of the coarse mode are mapped into sections 11–12 and 20–24 for the 12- and 24 section representations, respectively. Adjustments are made in the 4 km emissions of 11 key VOC and PM species by *Pun et al.* [2009] to ensure a consistency between the two sets of emissions at 12- and 4 km obtained from CARB. Emissions of long-chain alkanes and PAHs that are not treated in SAPRC are estimated as fractions of higher alkanes (ALK5) and aromatics based on information from CARB (P. Allen, CARB, Sacramento, CA, personal communication, 2006) and included as anthropogenic precursors to SOA. Emissions of biogenic species are distributed into individual species following *Helmig et al.* [1999]. The chemical initial and boundary conditions for gases and PM species provided by CARB are based on a CMAQ simulation at 12 km. These concentrations are set to be clean conditions over the Pacific Ocean for the 12 km simulation. For the 4 km simulation, the ICs for the first-day simulation are set to be the same as those for the 12 km simulation and those for the remaining days were taken from the last hour of the previous day, and the BCs for all simulation days were extracted from the 12 km simulation. The chemical initial and boundary conditions for PM are modified for the applications of MADRID 1 with 12 and 24 size sections by mapping those of Aitken and accumulation modes into fine and coarse size sections using the same approach as the distribution of emissions over size sections. More detailed description on model inputs and configurations can be found in the study of *Pun et al.* [2009]. Coagulation due to Brownian motion is included in the baseline simulations. Sensitivity simulations are also conducted without coagulation to study the impacts of coagulation on the simulated particle number concentrations and size distributions.

[7] The CRPAQS measurement data included in the evaluation are based on continuous 14 month annual (December 1999 through January 2001) measurements and 2 month winter (1 December 2000 through 3 February 2001) episodic measurements. The CRPAQS annual network includes three "anchor" monitoring sites measuring both gaseous and aerosol species and 53 supplemental "satellite" monitoring sites measuring aerosol species using portable monitors [*Watson et al.*, 1998]. The three anchor sites in the annual network are Angiola (ANG1), Bakersfield (BAC), and Fresno (FSF). While FSF and BAC represent urban areas in the central and southern portions of the SJV, respectively, ANGI, located in a remote agricultural area between FSF and BAC, represents rural areas. During the winter episodic field study, five additional sites (i.e., Bethel Island (BTI), Sacramento (SDP), San Jose (SJ4), Sierra Nevada Foothills (SNFH), and Walnut Grove Tower (WAG)) were upgraded from satellite to anchor sites. The site codes, names, types, coordinates, and chemical measurement data at these sites are provided in Table A1 in Appendix A. The CRPAQS site locations are shown in Figure 1. In addition to the 56 CRPAQS sites, measurements from the "backbone" network of CARB and air pollution control district sites

Figure 1. CMAQ−MADRID 1 modeling domain and observational sites during the California Regional $PM_{2.5}/PM_{10}$ Air Quality Studies (CRPAQS) listed in Table A1 (taken from http://www.arb.ca.gov/airways/crpaqs/siteAtlas/maps/CRPAQS_Labels.jpg).

are also included in the evaluation, as listed in Table A2 in Appendix A.

[8] Table 1 summarizes the type of data used in the evaluation, along with their sampling frequency, total number of sites, and site codes for all sites. The gaseous measurement data used for evaluation include hourly mixing ratios of carbon monoxide (CO), sulfur dioxide (SO_2), nitric oxide (NO), nitrogen dioxide (NO_2), total reactive nitrogen (NO_y), peroxyacyl nitrate (PAN), and O_3, 3–8 h average mixing ratios of nitric acid (HNO_3) and ammonia (NH_3), and 24 h average mixing ratios of NH_3. The PM mass measurement data include the 24 h average mass concentrations of $PM_{2.5}$ and its five major inorganic components (e.g., ammonium (NH_4^+), sulfate (SO_4^{2-}), nitrate (NO_3^-), EC, and OC) obtained using the Minivol filter sampler at 28–48 sites; the 5 times per day (3–8 h average) mass concentrations of $PM_{2.5}$ inorganic components obtained using the sequential filter sampler at three sites; the hourly mass concentrations obtained using the BAM-1020 sampler at eight sites; and 24 h average size-resolved mass concentrations obtained at two sites (ANGI and FSF) using the Micro Orifice Uniform Deposit Impactor (MOUDI) sampler for eight size stages over the size range of 0.056–10 μm (i.e., 0.056–0.1, 0.1–0.18, 0.18–0.32, 0.32–0.56, 0.56–1.0, 1.0–2.5, 2.5–5.62, and 5.62–10 μm). The

Table 1. Chemical Measurement Data Used in the Model Evaluation

Type	Sampling Method	Sampling Frequency	No. of Sites	Sampling Sites[a]
CO	Continuous CO analyzer	hourly	31	ARV, CA1, CCD, FCW, FSS, LOM, MAG, NAP, OKA, PBG, RED, SALH, SFA, SFEL, SOC, SPEP, SRF, SRL, TSM, UKG, VJO, WLM, BGS, BTI, CLO, FSD, LVR1, SFA, SJ4, SOH, VCS
SO_2	Continuous SO_2 analyzer	hourly	2	BAC,TRON
NO	Continuous NO analyzer	hourly	69	ARV, ATL, BSW, CA1, CCD, CCD, CRP, DVP, DVS, ECHO, ECP, EDS, ELK, FCW, FLN, FSS, GCL, GNF, GVB, LHS, LOM, LPD, LTY, LWP, M29, NAP, NAT, OJO, PBG, PLR, RED, ROS, SALH, SCFS, SFA, SHA, SLM, SMAR, SNH, SPEP, SRF, SRL, TEF, TPP, TRON, TSM, VBS, VICT, VJO, VIA, YAS, ANGI, BAC, BGS, BTI, CLO, FSD, FSF, HAN, LVR1, M14, MOP, OLD, S13, SDP, SFA, SJ4, SOH, VCS
NO_2	Continuous NO_2 analyzer	hourly	70	ARV, ATL, BSW, CA1, CCD, CCD, CRP, DVP, DVS, ECHO, ECP, EDS, ELK, FCW, FLN, FSS, GCL, GNF, GVB, LHS, LOM, LPD, LTY, LWP, M29, NAP, NAT, OJO, PBG, PLR, RED, ROS, SALH, SCFS, SFA, SHA, SLM, SMAR, SNH, SPEP, SRF, SRL, TEF, TPP, TRON, TSM, UKG, VBS, VICT, VJO, VIA, WLM, ANGI, BAC, BGS, BTI, CLO, FSD, FSF, HAN, LVR1, M14, MOP, OLD, S13, SDP, SFA, SJ4, SOH, VCS
HNO3	Sequential gas sampler with quartz/citric acid filter pack and citric acid denuder	3–8 h average, 5 times per day	3	ANGI, FSF, SNFH
NO_y	Continuous NO_y analyzer	hourly	3	ANGI, FSF, SNFH
PAN	Continuous PAN analyzer	hourly	3	ANGI, BAC, BTI
O_3	Continuous O_3 analyzer	hourly	51	ARV, BSW, CA1, CCD, CSS, DVS, ECHO, ECP, EDS, FSS, GVB, JAC, LMK, LOM, LTY, LWP, M29, MRA, PGN, PGV, PIRU, PLR, PRF, ROC, ROS, SCFS, SGS, SHA, SLM, SMAR, SNB, SYN, TPP, TRON, TSM, VICT, VIA, WCM, WLW, BAC, BGS, CLO, FSD, FSF, HAN, M14, MOP, OLD, S13, SOH, VCS
NH_3	Minivol sampler with Teflon/citric acid filter pack	24 h	21	ACP, BODB, BRES, CLO, COP, FEDL, FEL, FELF, FREM, FRES, HELM, LVR1, M14, MRM, OLW, PIXL, S13, SELM, SOH, SWC, VCS
	Sequential gas sampler with quartz/citric acid filter pack and citric acid denuder	3–8 h average, 5 times per day	3	ANGI, FSF, SNFH

Table 1. (continued)

Type	Sampling Method	Sampling Frequency	No. of Sites	Sampling Sites[a]
$PM_{2.5}$ mass	Minivol sampler with Teflon/citric acid filter pack	24 h	48	ACP, ALT1, BAC, BLI, BODB, BRES, BTI, CARP, CLO, COP, DOLA, DVL, EDI, EDW, FEDL, FEL, FELF, FREM, FRES, FSF, HELM, KAIS, KCG, KCW, LNP, LVR1, M14, MOP, MRM, OLD, OLW, PAC1, PIXL, PINN, PLE, PORE, S13, SELM, SEQU, SFA, SNFH, SRW, SOH, SWC, TEH2, TRIN, VCS, YOSE
	β attenuation monitor (BAM)-1020 sampler	hourly	8	ALT1, ANGI, BAC, BTI, FSF, SDP, SJ4, SNFH
$PM_{2.5}$ NH_4^+	Minivol sampler with quartz/NaCl filter pack	24 h	31	ACP, ANGI, BAC, BRES, BTI, CHL, CLO, COP, EDW, FEDL, FEL, FELF, FREM, FRES, FSF, HELM, LVR1, M14, MOP, MRM, OLD, OLW, PIXL, PLE, S13, SELM, SFA, SNFH, SOH, SWC, VCS
	Sequential filter sampler with quartz/Nacl filter pack	3–8 h average, 5 times per day	3	ANGI, FSF, SNFH
$PM_{2.5}$ SO_4^{2-}	Minivol sampler with quartz/NaCl filter pack	24 h	28	ACP, ANGI, BAC, BRES, BTI, CLO, COP, FEDL, FEL, FELF, FREM, FRES, FSF, HELM, LVR1, M14, MRM, OLD, OLW, PIXL, PLE, S13, SELM, SFA, SNFH, SOH, SWC, VCS
$PM_{2.5}$ NO_3^-	Minivol sampler with quartz/NaCl filter pack	24 h	31	ACP, ANGI, BAC, BRES, BTI, CHL, CLO, COP, EDW, FEDL, FEL, FELF, FREM, FRES, FSF, HELM, LVR1, M14, MOP, MRM, OLD, OLW, PIXL, PLE, S13, SELM, SFA, SNFH, SOH, SWC, VCS
	Sequential filter sampler with quartz/Nacl filter pack	3–8 h average, 5 times per day	3	ANGI, FSF, SNFH
	Continuous nitrate analyzer	hourly	7	ANGI, BAC, BTI, FSF, SJ4, SNFH, WAG
$PM_{2.5}$ EC	Minivol sampler with quartz/NaCl filter pack	24 h	31	ACP, ANGI, BAC, BRES, BTI, CHL, CLO, COP, EDW, FEDL, FEL, FELF, FREM, FRES, FSF, HELM, LVR1, M14, MOP, MRM, OLD, OLW, PIXL, PLE, S13, SELM, SFA, SNFH, SOH, SWC, VCS
	Continuous carbon analyzer	hourly	9	ANGI, BAC, BGS, FSF, M14, SDP, SJ4, SNFH, WAG
$PM_{2.5}$ OC	Minivol sampler with quartz/NaCl filter pack	24 h	31	ACP, ANGI, BAC, BRES, BTI, CHL, CLO, COP, EDW, FEDL, FEL, FELF, FREM, FRES, FSF, HELM, LVR1, M14, MOP, MRM, OLD, OLW, PIXL, PLE, S13, SELM, SFA, SNFH, SOH, SWC, VCS
	Continuous carbon analyzer	hourly	2	ANGI, BAC
PM size distribution and number concentrations	Micro Orifice Uniform Deposit Impactor (MOUDI) sampler (i.e., the mass concentrations of PM components in 8 size stages and derived number concentrations).	5–8 h average, 1–2 times per day	2	ANGI, FSF

[a]The full names of the monitoring sites can be found in Tables A1 and A2 in Appendix A.

Table 2. Performance Statistics for Gaseous Species and PM and Its Components

Species[a, b]		Obs. (ppb or μg m^{-3})[a]	Sim. (ppb, μg m^{-3})[a]	Data Pair	R[c]	NMB[c] (%)	NME[c]
CO	12 s[b]	1528.23	474.80	4113	0.31	−68.9	69.6
NO	12 s	48.52	9.28	9168	0.24	−80.9	90.3
NO_2	12 s	20.56	16.13	10569	0.53	−21.5	51.8
NO_y	12 s	58.62	21.65	481	0.70	−63.1	66.9
PAN	12 s	0.14	0.26	208	0.60	73.9	90.5
SO_2	12 s	1.64	1.75	266	−0.02	6.9	69.7
O_3	12 s	16.77	24.64	7755	0.55	46.9	72.5
NH_3	12 s	0.06	0.04	60	−0.07	−29.2	1.12
$PM_{2.5}$	12 s	34.01	31.91	142	0.88	−6.2	28.3
	24 s		34.18	142	0.88	0.5	28.9
NH_4^+	12 s	4.23	5.03	94	0.70	18.7	44.7
	24 s		5.23	94	0.70	23.6	48.2
SO_4^{2-}	12 s	1.44	1.15	93	0.45	−19.7	44.3
	24 s		1.36	93	0.39	−5.1	50.7
NO_3^-	12 s	12.34	16.29	92	0.69	32.1	53.0
	24 s		17.30	92	0.69	40.2	59.0
EC	12 s	1.91	2.60	96	0.70	35.8	54.4
	24 s		2.62	96	0.71	36.8	54.7
OM	12 s	17.21	5.68	96	0.74	−67.0	68.6
	24 s		5.70	96	0.74	−66.9	68.5
NUM	12-nocoag	22294.4	48715.19	10	0.074	118.5	120.8
	12-coag		17432.54	10	0.46	−21.8	46.7
	24-nocoag		55093.17	10	0.074	147.1	147.1
	24-coag		19205.80	10	0.46	−13.9	44.9

[a]The unit for gaseous and PM concentrations are ppb and μg m^{-3}, respectively. The statistics for gas-phase species are only shown for the CMAQ simulation with 12 sections, which is very similar to those with 24 sections.

[b]The statistics are calculated based on hourly mixing ratios of gases except for NH_3 for which only observed 24 h average mixing ratios were available at 21 sites for model evaluation, based on 24 h average concentrations for $PM_{2.5}$ and its components obtained using the Minivol sampler at 48 sites, and based on the derived PM_{10} number concentrations obtained using the eight stage MOUDI sampler during the five sampling time periods at two sites (see Table 3). The data on after-filter (<0.056 μm) were excluded.

[c]sec, section; R, correlation coefficient; NMB, normalized mean bias; NME, normalized mean error.

MOUDI after-filter (<0.056 μm) data are excluded due to extremely high concentrations of EC and OC that may be subject to errors and uncertainties [*Chow et al.*, 2008]. These observations were obtained using different methods by different investigators and may not be internally consistent even at the same sites due to limitations and uncertainties in these methods. Such inconsistencies and associated uncertainties will be discussed along with specific comparisons later. Both hourly and 24 h average EC/OC measurements used in this study were analyzed based on the Interagency Monitoring of PROtected Visual Environments (IMPROVE) protocol (i.e., a thermo-optical reflectance (TOR) protocol) [*Watson et al.*, 1998; *Chow et al.*, 2006; *Ying et al.*, 2008b], which gives different EC and OC definitions from the model simulation that uses the emission data base based on the NIOSH method. Before comparing with simulated EC and OM concentrations, the observed EC and OC concentrations are therefore adjusted to be consistent with the NIOSH system by transferring 50% of the observed EC into observed OC concentrations, which are then converted to OM concentrations by multiplying by a factor of 1.4, following the approach of *Held et al.* [2004] and *Ying et al.* [2008b]. Simulated gaseous and PM mass concentrations are evaluated in terms of spatial distributions, temporal variations (daily and hourly), and domain-wide statistics. Simulated PM size distributions from 12 and 24 sec simulations are mapped into the eight size stages to compare with observed size distributions. Simulated PM number concentrations are evaluated in terms of spatial distributions, 5–8 h average over the eight size stages and the full size range at specific sites, and statistics using the PM number concentrations derived from the observed size-resolved mass concentrations for the eight size stages. A density of 1.35 g cm^{-3} is used to convert the Stokes diameter used in the model simulations to the aerodynamic diameter used in the observations for comparison, following *Zhang et al.* [2004]. Although a portion of the PM in the Central Valley is soil dust that has a density of 2.3–2.7 g cm^{-3} [e.g., *Blanco-Canqui et al.*, 2006], soil dust emission is not included in this version of CMAQ-MADRID. Since such size-resolved PM component measurements do not include other unknown inorganic PM (OIN) and the MOUDI after-filter data are excluded, the derived number concentrations may somewhat underestimate the actual observed PM number concentrations.

3. Model Results and Discussions

3.1. Evaluation of Mass Concentrations of Gases

[9] While the winter O_3 mixing ratios are generally not a concern for the attainment of NAAQS in CA, their analyses along with relevant gaseous species can indicate the accuracy of emissions used and meteorology simulated, which in turn affects PM predictions because O_3 and $PM_{2.5}$ are affected by the same set of meteorological variables and share some common gaseous precursors such as nitrogen oxides (NO_x = NO + NO_2) and VOCs. Table 2 shows domain-wide performance statistics for the 24 h average concentrations of NH_3 and hourly concentrations of other gases. The concentrations of CO, NO, NO_2, NO_y, and NH_3 are moderately to significantly underpredicted with normalized mean biases (NMBs) of −80.9% to −21.5%. The concentrations of SO_2, PAN, and O_3 are overpredicted with NMBs of 6.9%–73.9%. In addition to uncertainties in emissions and meteorology, the high concentrations of PAN and O_3 can be partially attributed to the inclusion of higher aldehydes and relevant oxidation re-

actions; the lack of photolytic reaction for PAN in SAPRC99 may also contribute to the overestimate of PAN. Analyses of emissions and measured ambient concentrations suggest that the CRPAQS emission inventory underestimates the emissions of CO and VOCs as well as early morning (05–07 Pacific Standard Time (PST)) emissions of NO_x from area sources but overestimates primary emissions of $PM_{2.5}$ and slightly overestimates the early morning emissions of SO_2 [*Raffuse and Chinkin*, 2005]. NH_3 emissions may also be underestimated for most sites. Using the same CARB-generated emissions but diagnostic meteorological fields and a different 3-D air quality model, *Ying et al.* [2008b] reported that missing combustion sources may contribute to the undepredicted concentrations of CO, NO, EC, and OC, particularly at ANGI. The inaccuracies and uncertainties in the emission inventories may be due to the misclassification or exclusion of major emissions sources, the use of incorrect emissions activity data, emission factors, and chemical speciation profiles, as well as uncertainties in the emission modeling [*Raffuse and Chinkin*, 2005; *Livingstone et al.*, 2009]. In addition, inaccuracies in meteorological predictions (e.g., wind fields) also affect the predictions of gaseous and PM species.

[10] Figure 2 shows hourly variations of O_3 at seven CRPAQS sites (i.e., BAC, Clovis (CLO), Fresno (FSF), Modesto (M14), Mojave (MOP), Sacramento (S13), and Stockton (SOH)) and seven CARB backbone sites (i.e., Capitan (CA1), Gaviota (GVB), Placerville (PGN), Pleasant Grove (PGV), Victorville (VICT), Ventura (VIA), and White Cloud Mountain (WCM)). Among these, seven are urban sites representing a wide geographic coverage in different portions of SJV (northern: M14 and SOH, central: CLO and FSF, and southern: BAC) and adjacent Air Basins including the North Central Coast (S13) and the South Central Coast (CA1). BAC, FSF, M14, S13, and SOH are sites established during CRPAQS to determine community exposure to $PM_{2.5}$ in urban areas and CLO represents a source area in the central SJV. PGN is located in the Sierra Nevada foothills in the north of SJV and represents rural areas. PGV is also located in the north of SJV and represents rural and agricultural areas. MOP represents rural and desert areas in the southeast of SJV. Two sites are selected to represent coastal areas: GVB, an elevated site (305 m mean sea level (msl)) in the southwest of SJV and VIA, an elevated site (319 m msl) is located in Ventura County in the south of SJV. Two sites in the east of SJV are selected to represent mountain areas: VICT (876 m msl) is located at the southern edge of the Mojave Desert in western San Bernardino County and WCM (1320 m msl) is located in Bishop, flowing out of the Sierra Nevada. As shown in Figure 2, the observed daily peak O_3 concentrations at urban sites are in the range of 10–50 ppb, with the higher values occurring in the central or southern portions of SJV (i.e., CLO, BAC, FSF) or south of SJV (i.e., CA1) and lower values occurring in the northwest of SJV (i.e., S13) or in the northern portion of SJV (i.e., SOH and M14). Observed O_3 concentrations started to build up due to increased local emissions during the Christmas and New Year Holiday's at BAC, CLO, and FSF. While the model is able to capture the daytime variation and the correct peak O_3 hours at these sites as well as the differences in temporal variations between urban inland and coastal sites, it significantly underpredicts the observed peak O_3 concentrations due most likely to the underestimation of precursor emissions at BAC, CLO, and FSF. The model significantly overpredicts daily O_3 concentrations at S13 due likely to an underestimate of mixing heights (thus ventilation rates) around this site and nighttime/early morning O_3 at several sites (e.g., BAC, CLO, S13, SOH, VICT, GVB) due likely to a lack of NO titration as a result of underestimated NO emissions during morning and evening hours and possible underestimate in early morning mixing heights. The overpredictions in nighttime O_3 occur on many days at nearly all urban sites (except for CA1 where the O_3 diurnal profile is different from that inland due to the impact of sea breezes and offshore wind flows), further confirming domain-wide underestimated NO emissions. The model performs well at all mountain and coastal sites (i.e., VICT, WCM, GVB, and VIA) and one rural site (i.e., PGN) but fails to reproduce nighttime O_3 at PGV and MOP where NO concentrations could have been significantly underestimated, which has been confirmed by comparing simulated NO mixing ratios with observations at MOP (figure not shown). The inaccurate NO_x mixing ratios will affect next-day's O_3 and OH mixing ratios, which will in turn affect the formation of secondary $PM_{2.5}$.

3.2. Evaluation of Mass Concentrations of PM Species

[11] Figure 3 shows the spatial distributions of simulated weekly mean mass concentrations of $PM_{2.5}$ and its five major components from the 12 sec simulation, overlaid with available observations. Those from the 24 sec simulation are similar, thus not shown. The corresponding domain-wide statistics for 12 and 24 km simulations are given in Table 2. Overall, the model is able to capture the spatial variations and magnitudes of $PM_{2.5}$ concentrations in the SJV, with higher values occurring in the central and southern portions of the SJV and lower values in the north and northern portions of the SJV as well as the adjacent mountain and coastal areas, consistent with observations during CRPAQS [*Chow et al.*, 2006]. The underpredictions and overpredictions at some sites compensate each other, leading to small NMBs of −6.5% and 0.5% for the 12 and 24 km simulations, respectively. SO_4^{2-} concentrations are well simulated in the northern and central portions of SJV but underpredicted in the southern portion of SJV, with domain-wide NMBs of −19.7% and −5.1% for the 12 and 24 sec simulations, respectively. NH_4NO_3 dominates $PM_{2.5}$; its spatial distribution follows closely with that of $PM_{2.5}$, with high concentrations spreading out a large area in the central and southern portions of the SJV where overpredictions of NO_3^- and NH_4^+ occur. The NMBs are 32.1% and 18.7% for the 12 sec simulation and 40.2% and 23.6% for the 24 sec simulation, respectively. The differences in simulated SO_4^{2-}, NO_3^-, and NH_4^+ between 12 and 24 sec simulations are due mainly to differences in the gas/particle mass transfer rates and the dry deposition rates that are size dependent. The overpredictions in NH_4^+ and NO_3^- may indicate the inaccuracy in the emissions of NH_3 and/or NO_x and inappropriate gas/particle partitioning of total nitrate and ammonium. Observed OM concentrations are significantly underpredicted at most sites in the SJV with NMBs of −67% for both simulations. While the underpredictions in OM are clearly associated with the underestimates in primary $PM_{2.5}$ emissions, the underpredictions in SO_4^{2-} may be caused by several factors including inaccuracy in the emissions of SO_2 and primary SO_4^{2-}, the

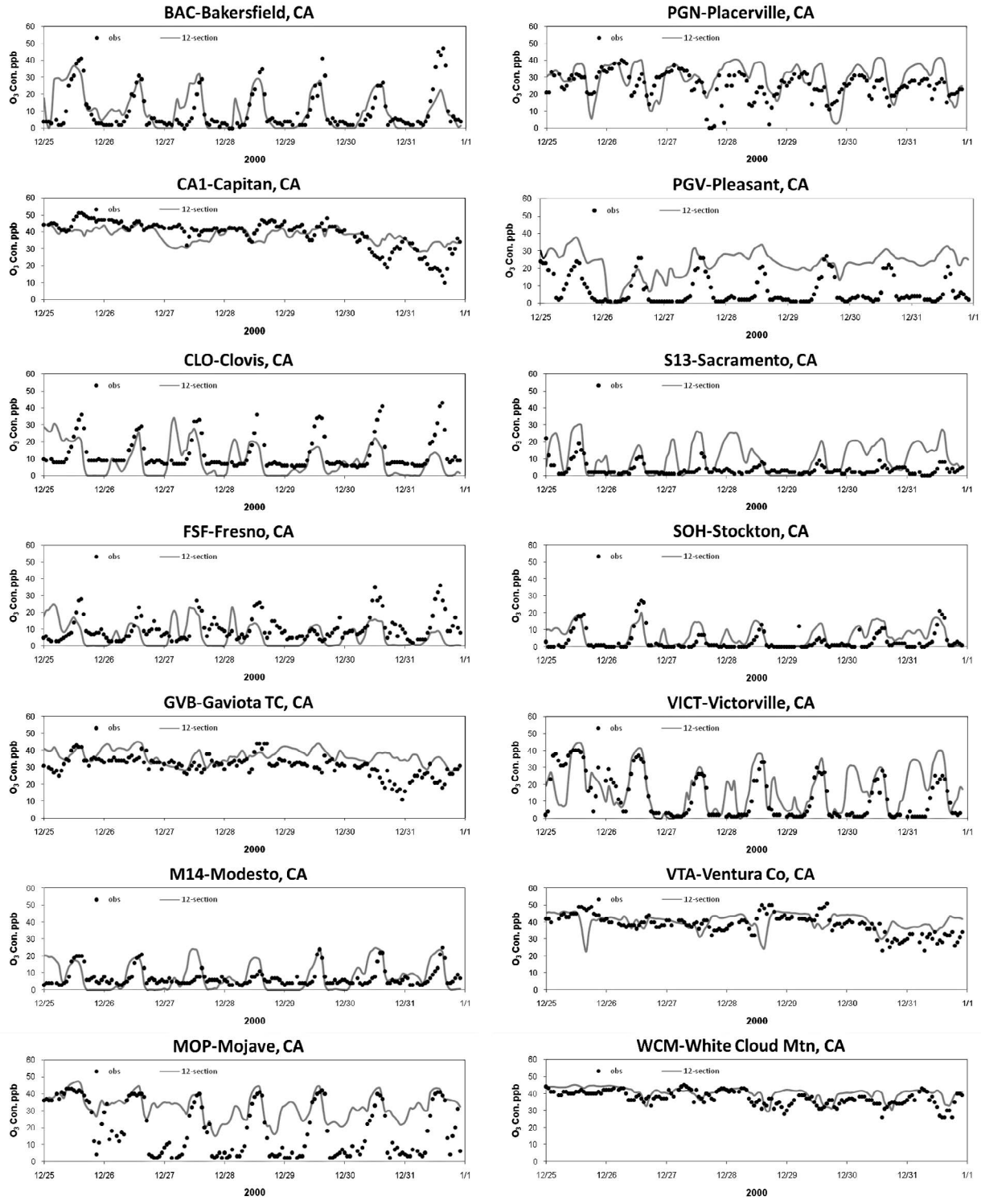

Figure 2. Temporal variations of O_3 at 14 CRPAQS sites and CARB backbone sites during 25–31 December 2000.

gas- and aqueous-phase chemistry treated, and the simulated meteorological fields (e.g., solar radiation, temperature, and cloud/fog events captured). Different from the study of *Ying et al.* [2008b], 24 h average EC concentrations are overpredicted throughout the SJV, with NMBs of 35.8% and 36.8% for the 12 and 24 sec simulations, respectively, despite potential underestimates in EC emissions indicated by *Ying et al.* [2008b]. This may indicate uncertainties in other factors such as vertical mixing and dry deposition that may affect simulated BC concentrations and distributions. For example,

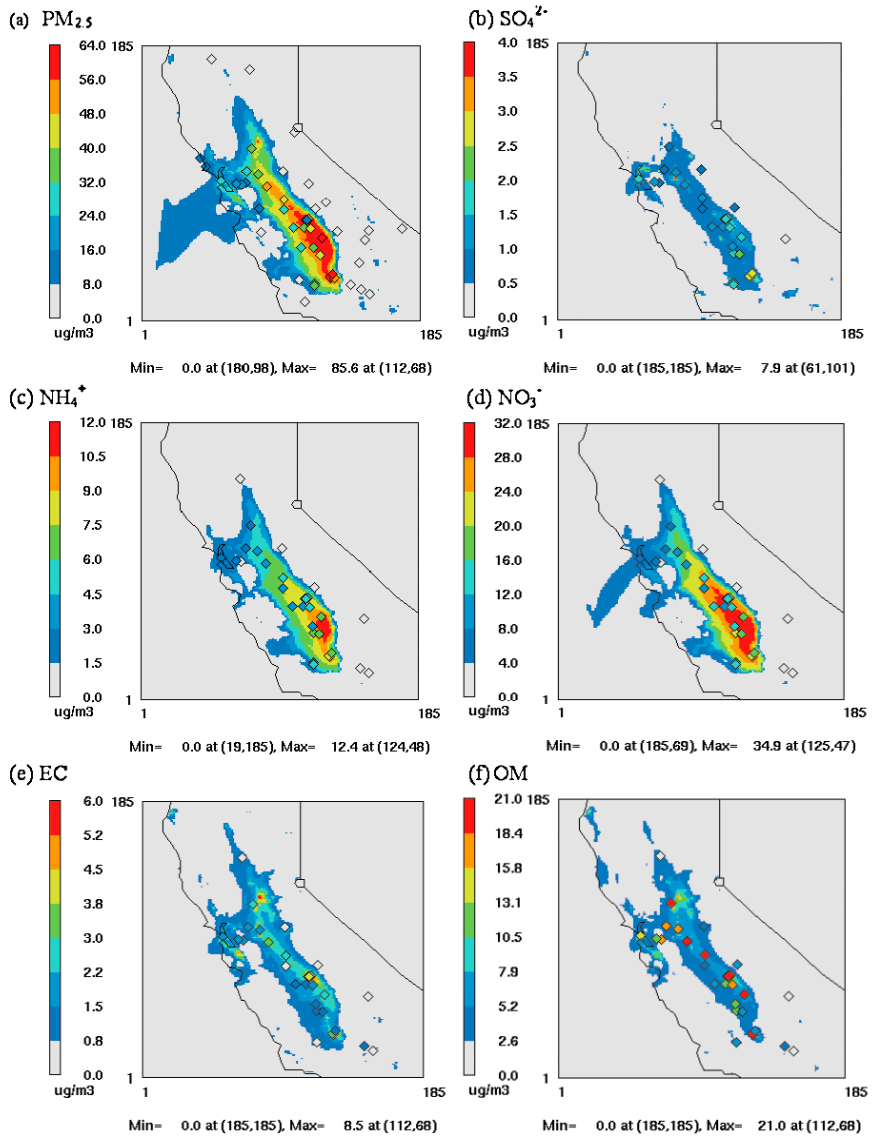

Figure 3. Overlay of observed and simulated spatial distributions of weekly mean mass concentrations of $PM_{2.5}$ and its major components from the 12 and 24 sec simulations with coagulation during 25–31 December 2000.

the simulated daytime mixing heights of 100–500 m are generally lower than the observed values of 500–1000 m in most areas in winter in the SJV reported by *MacDonald et al.* [2003], leading to the overpredictions in the EC concentrations. Similar to the SO_4^{2-} predictions, the high concentrations of EC and OM occur at a few urban sites, which is different from the more homogeneous distributions of NH_4NO_3 in urban and rural areas throughout the SJV. Such differences in the spatial distributions of EC/OM and NH_4NO_3 are attributed to differences in their formation mechanisms. For example, primary OM and EC emissions from urban areas and limited dispersion under winter stagnant conditions dominate the spatial distributions of OM and EC particles, whereas daytime photochemistry and subsequent condensation of HNO_3 and NH_3 in the PBL and nighttime nitrogen chemistry aloft dominate the formation and distribution of NH_4NO_3 [*Neuman et al.*, 2003; *McCarthy et al.*, 2005; *MacDonald et al.*, 2003].

[12] The 24 h average concentrations of $PM_{2.5}$ and its components were measured at 48 and 28–31 sites, respectively, but most of them having no concurrent O_3 measurements. Figure 4 shows the simulated and observed 24 h average concentrations of $PM_{2.5}$ and its major components on 26 December at 14 sites. High 24 h average $PM_{2.5}$ concentrations of 20–73 $\mu g\ m^{-3}$ were observed at urban sites throughout the SJV (from the highest to the lowest: FSF, BAC, CLO, M14, and SOH) and adjacent air basins (S13, San Francisco (SFA), Livermore (LVR1)). High observed $PM_{2.5}$ concentrations of 22–30 $\mu g\ m^{-3}$ also occurred at three rural sites (BTI, Pixley National Wildlife Refuge (PIXL), and Pleasant Grove (PLE)). At MOP and the Sierra Nevada Foothills sites (SNFH and Olancha (OLW)), the observed

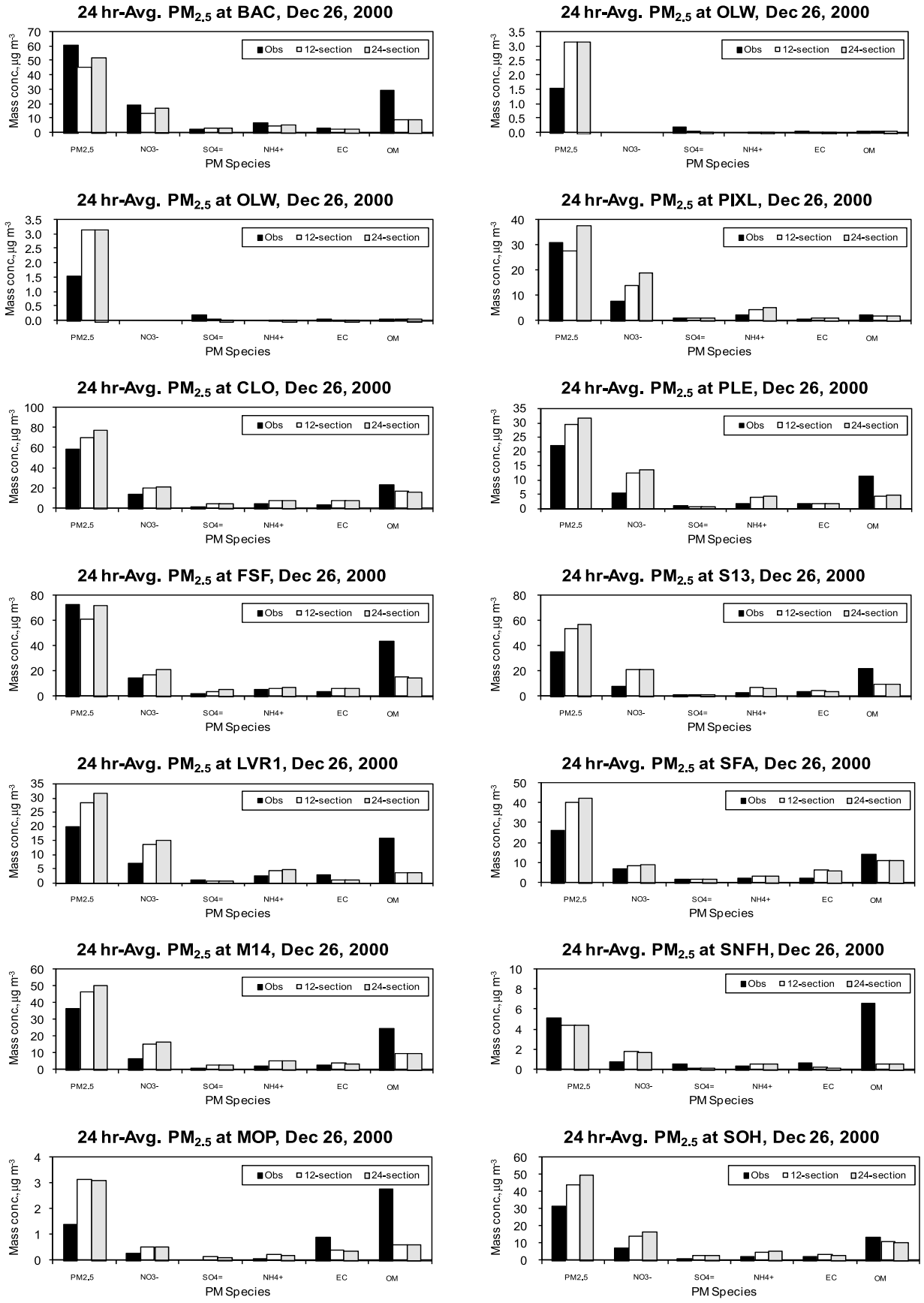

Figure 4. Observed versus simulated 24 h average mass concentrations of $PM_{2.5}$ and its components at 14 CRPAQS sites and CARB backbone sites on 26 December 2000.

$PM_{2.5}$ concentrations were below 5.2 $\mu g\ m^{-3}$, representing background concentrations in the region. The model tends to overpredict $PM_{2.5}$ concentrations throughout the domain at all these sites except for SNFH on 26 December but underpredictions dominate at most sites on 25 and 28 December (Figures not shown) and compensate the overpredictions, resulting in a small domain-wide NMB of −6.2% to 0.5%. As expected, NO_3^-, NH_4^+, OM, and EC are the major components of $PM_{2.5}$ at these sites. The observed SO_4^{2-} concentrations are slightly overpredicted at most sites on this day. Significant underpredictions in OM occur at all sites except for SFA, SOH, PIXL, and OLW, reinforcing the hypothesis of a domain-wide underestimate in the emissions of primary OM. EC concentrations are either overpredicted or underpredicted. The overpredictions in major PM components NO_3^- and NH_4^+ at most sites and in OIN (figure not shown) at BAC, SFA, and FSF dominate over the underpredictions in OM, causing an overall overprediction in $PM_{2.5}$ on 26 December. Since the 24 h concentrations of $PM_{2.5}$ and its components were measured using the same type of sampler (i.e., the Minivol sampler) but with different filter packs (see Table 1), their concentrations may not be self-consistent. For example, the sum of the concentrations of the 5 $P.M._{2.5}$ components is much higher than that of $PM_{2.5}$ at LVR1, SNFH, and MOP, indicating a likely mass loss in the total $PM_{2.5}$ mass samples taken at these sites.

[13] The concurrent measurements of NH_3, HNO_3, NH_4^+, and NO_3^- are only available on 26–28 December at three sites: ANGI, FSF, and SNFH; they were obtained using a different method as the 24 h average concentrations (i.e., the sequential filter sampler, instead of the Minivol filter sampler) and thus may not be consistent with the 24 h average concentrations shown in Figure 4. For example, the concentrations of NH_4^+ and NO_3^- using the sequential filter sampler are higher than those using the Minivol sampler shown in Figure 4 at FSF and SNFH, indicating less mass loss due to volatility and thus better accuracy in the measurement data obtained with the sequential filter sampler. The measurements of NH_3 and HNO_3 were made using the sequential gas sampler with quartz/citric acid filter pack and citric acid denuder, which is also different from the Minivol sampler used for the 24 h average concentrations of NH_3. Nevertheless, these concurrent measurements provide insights into the observed partitioning of total ammonium ($TNH4 = NH_3 + NH_4^+$) and total nitrate ($TNO3 = HNO_3 + NO_3^-$) in the gas and particulate phases. Figure 5 shows the simulated versus observed TNO3 and TNH4 at these sites. Underprediction that dominates the simulated TNO3 at these sites (except for 28 December at FSF and 26 December at SNFH), coupled with the fact that most TNO3 exist as NO_3^- during winter, supports a dominance of the underestimate in NO_x emissions among all likely factors causing this underprediction. For TNH4, a significant underprediction on all days at ANGI and overprediction at FSF indicate underestimate and overestimate, respectively, of NH_3 emissions at those sites. In addition, TNH4 exists mostly as NH_3 at ANGI and SNFH and >41% at FSF due to a lack of NO_3^- and SO_4^{2-} for their neutralization at these sites, indicating a NO_x-limited (rather than NH_3-limited) NO_3^- formation at these sites. These results are qualitatively consistent with the observed abundance of NH_3 and low concentrations of HNO_3 during winter episodes in this region reported by other studies (e.g., *Kumar et al.*, 1998; *Pun and Seigneur*, 1999, 2001; *Watson and Chow*, 2002; *Herner et al.*, 2005].

[14] Figure 6 compares simulated hourly $PM_{2.5}$ concentrations with those observed using the BAM-1020 sampler at the eight CRPAQS sites, each serving different purposes during CRPAQS. While BAC, FSF, San Jose-4th Street (SJ4), and Sacramento-Del Paso Manor (SDP) are four urban sites to determine community exposure to $PM_{2.5}$ during the CRPAQS, Altamont Pass (ALT1) and BTI are established to provide insight into the transport of air masses between the Bay Area and the Central Valley (i.e., interbasin study), and ANGI and SNFH are sites to study intrabasin transport and vertical gradient. As time approached the end of the year, the buildup of concentration is evident from observations at all urban and rural sites except for ALT1 and BTI, as a result of the combined effect of increased local emissions due to the Christmas and New Year Holiday's and a strong stagnation event with strong stability aloft that led to limited mixing and light wind flow during afternoon hours. The passage of a cold front with 0.10 inches of rainfall to Bakersfield on 20 December created a moist atmosphere with relative humidities of 85%–100% along with light fog and haze in the morning across the SJV [*Ferreria and Shipp*, 2005]. These cool damp mornings with moisture favored the formation of NH_4NO_3 and SOA. The peak $PM_{2.5}$ concentrations occur at night and early morning, indicating that nighttime chemistry may have played a role in the NH_4NO_3 formation [*Neuman et al.*, 2003; *McCarthy et al.*, 2005]. The $PM_{2.5}$ concentration buildup trend and the dominance of NH_4NO_3 at ANGI are similar to those of FSF and BAC, clearly indicating regional transport of pollutants. Compared with other sites, the observed concentrations are lower at ALT1, BTI, and SNFH. The low concentrations at these sites reflect a low vertical mixing as a result of weak PBL turbulence during high $PM_{2.5}$ days [*Chow et al.*, 2006]. The model is able to capture the overall buildup trends and magnitudes of $PM_{2.5}$ concentrations at ANGI, BAC, and FSF but fails to reproduce the diurnal variations. The model reproduces well $PM_{2.5}$ concentrations during some periods at ALT1, SJ4, SDP, and BTI, although large underpredictions occur during 30–31 December at ALT1, SJ4, and BTI and during most of time at SNFH and SDP, due likely to the underestimates in primary OC emissions and an underestimate of NO_x emissions at either sites located at/near sources (e.g., SJ4) or underestimates in EC and OC concentrations at nonsource sites (e.g., SNFH) that are affected by interbasin transport from upwind sites. At all sites, 12- and 24 section simulations give similar $PM_{2.5}$ temporal variation trends. As shown in Figure 7, hourly NO_3^- concentrations are largely overpredicted at ANGI and FSF during most days and nights and at SJ4 and WAG during some nights/mornings, contributing to most of the overpredictions during nighttime/morning $PM_{2.5}$ concentrations at ANGI, FSF, and SJ4 (see FSF in Figure 4). The diurnal variations of NO_3^- are well reproduced at SNFH but its concentrations are underpredicted, which helps explain the underpredictions in the 24 h average $PM_{2.5}$ concentrations at this site shown in Figure 4. The model performs well in terms of capturing magnitudes and buildup trends of NO_3^- concentrations at BAC although an opposite temporal trend exists between simulations and observations. While the overall lower simulated daytime values at most

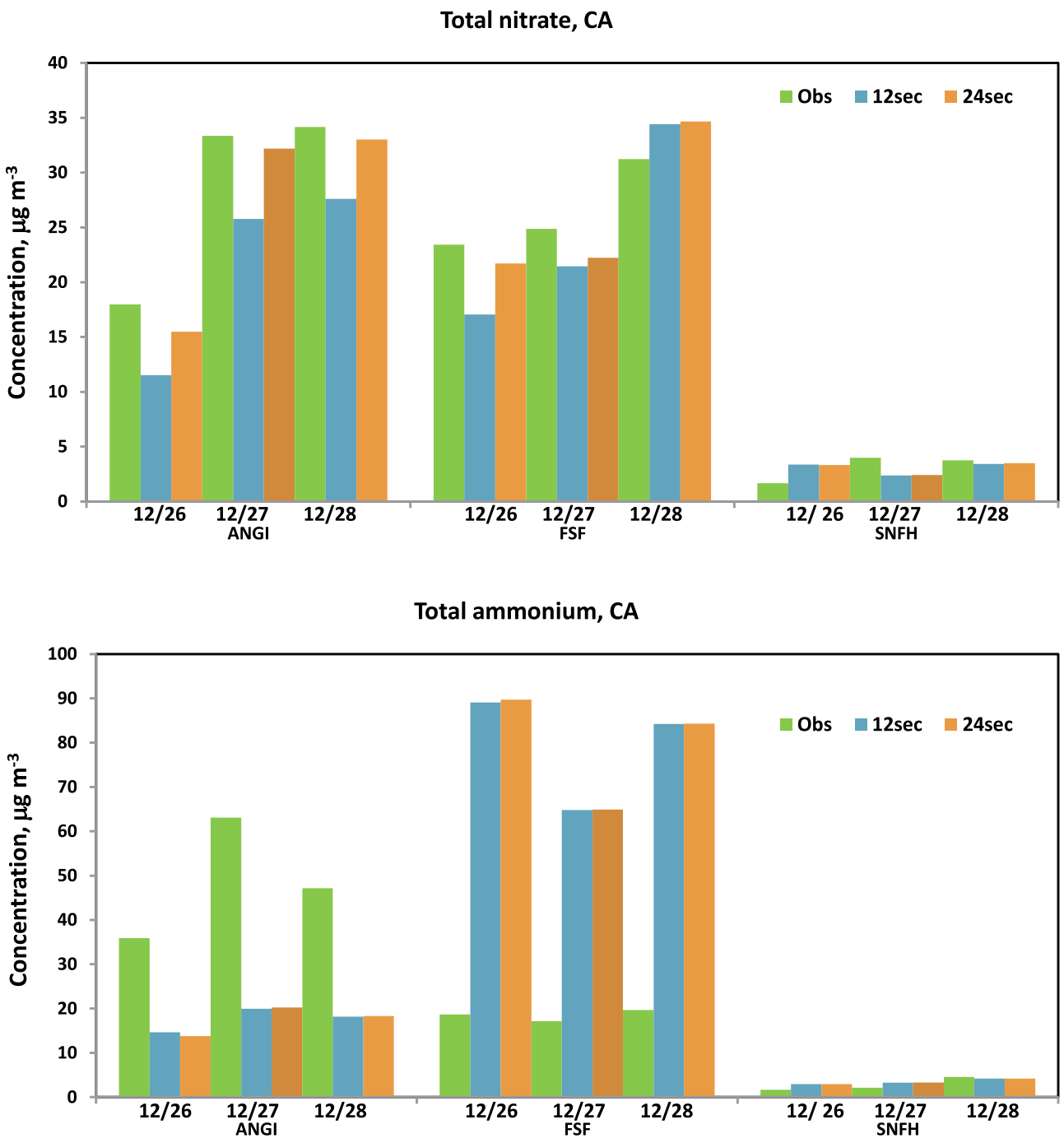

Figure 5. Total nitrate and total ammonium at ANGI, FSF, and SNFH during 26–28 December 2000.

sites may be caused by lower NO_x emissions and weaker photochemistry than observed, the higher NH_4NO_3 concentrations during night/morning hours may be caused by too fast heterogeneous chemical formation of HNO_3 through reactions of NO_3 and N_2O_5 at night, inappropriate gas/particle partitioning that places too much nitrate in the particulate phase and cold biases in simulated winter temperatures. *Pun et al.* [2009] examined the sensitivity of NO_3^- formation and found that the heterogeneous reaction in CMAQ-MADRID accounted for about two thirds of the nitrate production at rural sites and more at urban sites during peak periods. The heterogeneous reaction probability value (i.e., uptake coefficient) for N_2O_5 used in this study is 0.1, which represents an upper estimate [*Evans and Jacob*, 2005]. The same value was used in CMAQ v4.2.2 or older, leading to significant overpredictions in NO_3^- formation over both the western and eastern United States, particularly in winter [*Bhave et al.*, 2006; *Gilliland et al.*, 2006]. Depending on temperature, RH, and types and chemical compositions of the surfaces, the reported values from laboratory measurements range from 0.002 to 0.08 [*Davis et al.*, 2008 and references therein], which are much lower than the value of 0.1 in this study. The latest version of CMAQ (v4.7) uses the parameterization of *Davis et al.* [2008], which calculates uptake coefficient of

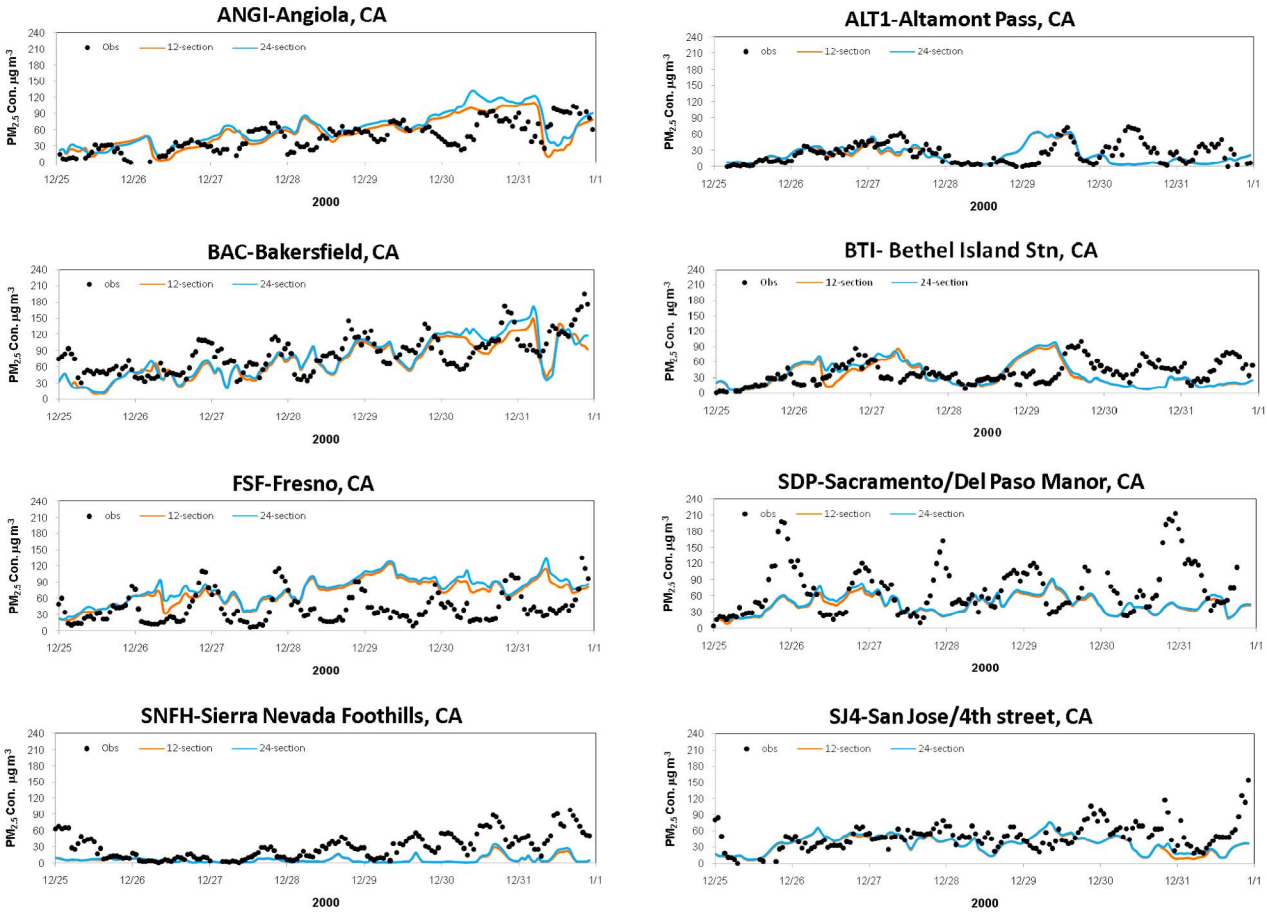

Figure 6. Temporal variations of $PM_{2.5}$ mass concentrations at eight sites during 25–31 December 2000.

N_2O_5 as a function of temperature, RH, particle composition, and phase state (e.g., aqueous versus solid particles) based on a regression fitting equation that reproduces 80% of laboratory measurements within a factor of two, providing a more realistic uptake coefficient of N_2O_5. Hourly EC concentrations are overpredicted at all sites except at SNFH. Primary OM concentrations dominate simulated OM concentrations due to limited photochemical oxidation that dictates SOA formation under the winter conditions. While hourly OM concentrations are underpredicted at ANGI, they are overpredicted at BAC. However, the observed hourly OM concentrations are only available at two sites: ANGI and BAC, limiting a complete assessment of the model's ability in simulating hourly variation of OM. It is noted that a significant inconsistency in observations exists for some species between their hourly concentrations measured by the continuous carbon analyzer and the 24 h concentrations measured by the Minivol sampler. For example, the observed 24 h average and hourly EC and OM concentrations shown in Figures 4 and 7 at BAC are not consistent, leading to an inconsistent model performance assessment at this site using these observations. In particular, the observed hourly OM concentrations are lower by about a factor of 3 than the 24 h average concentrations. Similarly, the observed hourly NO_3^- concentrations shown in Figure 7 are much lower than the 24 h average concentrations shown in Figure 4 at BAC. This indicates some uncertainties associated with the OM and NO_3^- measurements, which contain volatile mass and thus are difficult to measure. As shown in section 3.3, the size-resolved PM component measurements during certain time periods using the MOUDI with Teflon, ion chromatography, and automated colorimetry also show high concentrations of OM in the fine PM size sections at ANGI and FSF (see Figure 8), which seems more consistent with the 24 h average concentrations measured by the Minivol sampler than the carbon analyzer. The concentrations of EC and OM from the 12 and 24 section simulations are similar at all sites but those of NO_3^- are somewhat different during some periods at some sites (e.g., during some day hours at ANGI, BAC, and FSF on December. Twenty six and at ANGI and BAC on 31 December), indicating some numerical instability in the gas/particle partitioning treatment in ISORROPIA used in CMAQ. Specifically, NO_3^- concentrations suddenly dropped to very low values in the 12 sec simulation. This is likely due to a simplified approach used in ISORROPIA to solve gas/particle thermodynamic equilibrium equations that are based on three chemical regimes: sulfate rich, neutral, and poor (instead of a continuous regime). This may cause a discontinuity in the solution under some conditions when a coarse size resolution is used. As shown in Figure 7, the use of a finer size resolution, such as 24 size sections, gives a more robust solution in gas/particle partitioning.

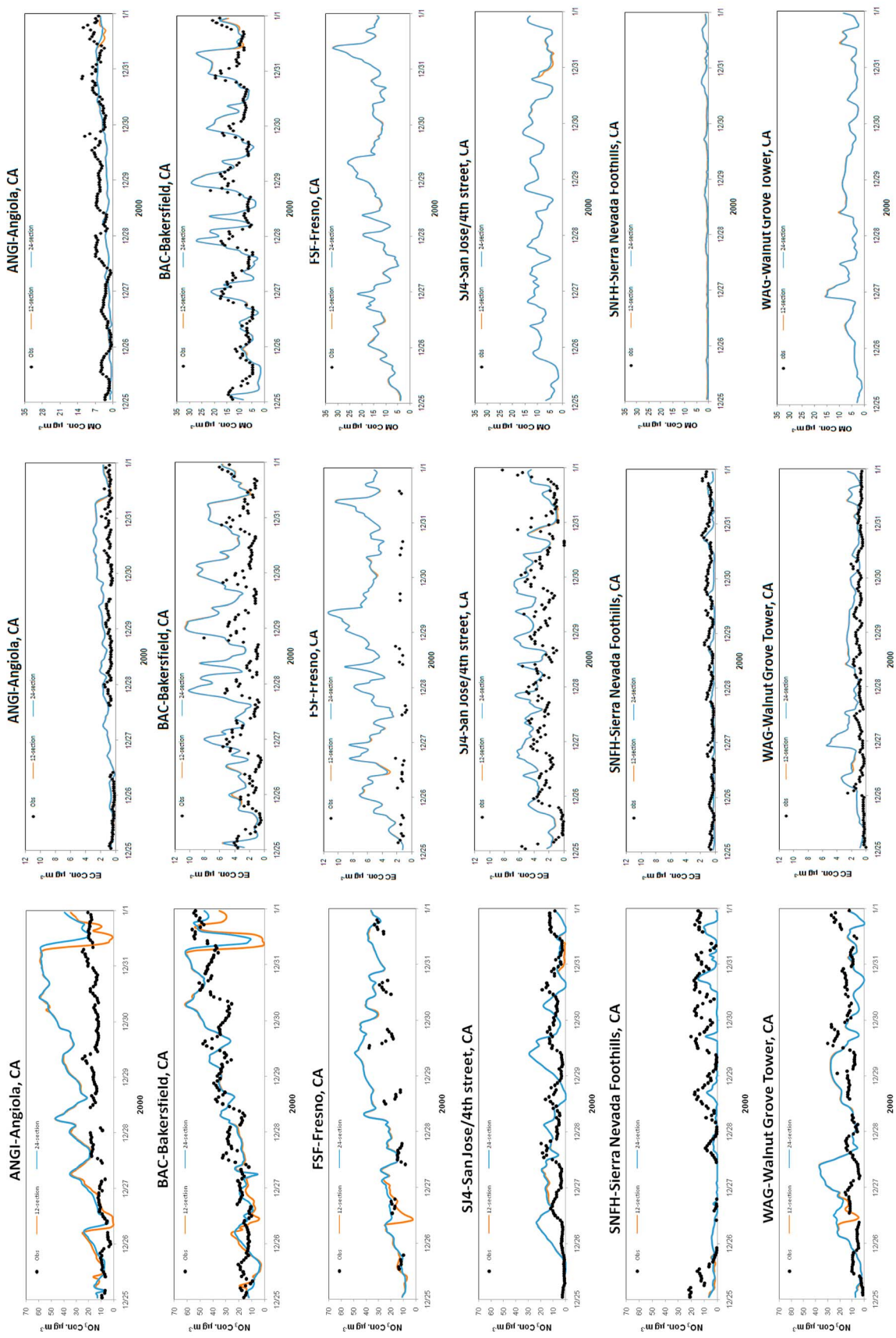

Figure 7. Temporal variations of mass concentrations of $PM_{2.5}$ NO_3^-, EC, and OM at six sites during 25–31 December 2000.

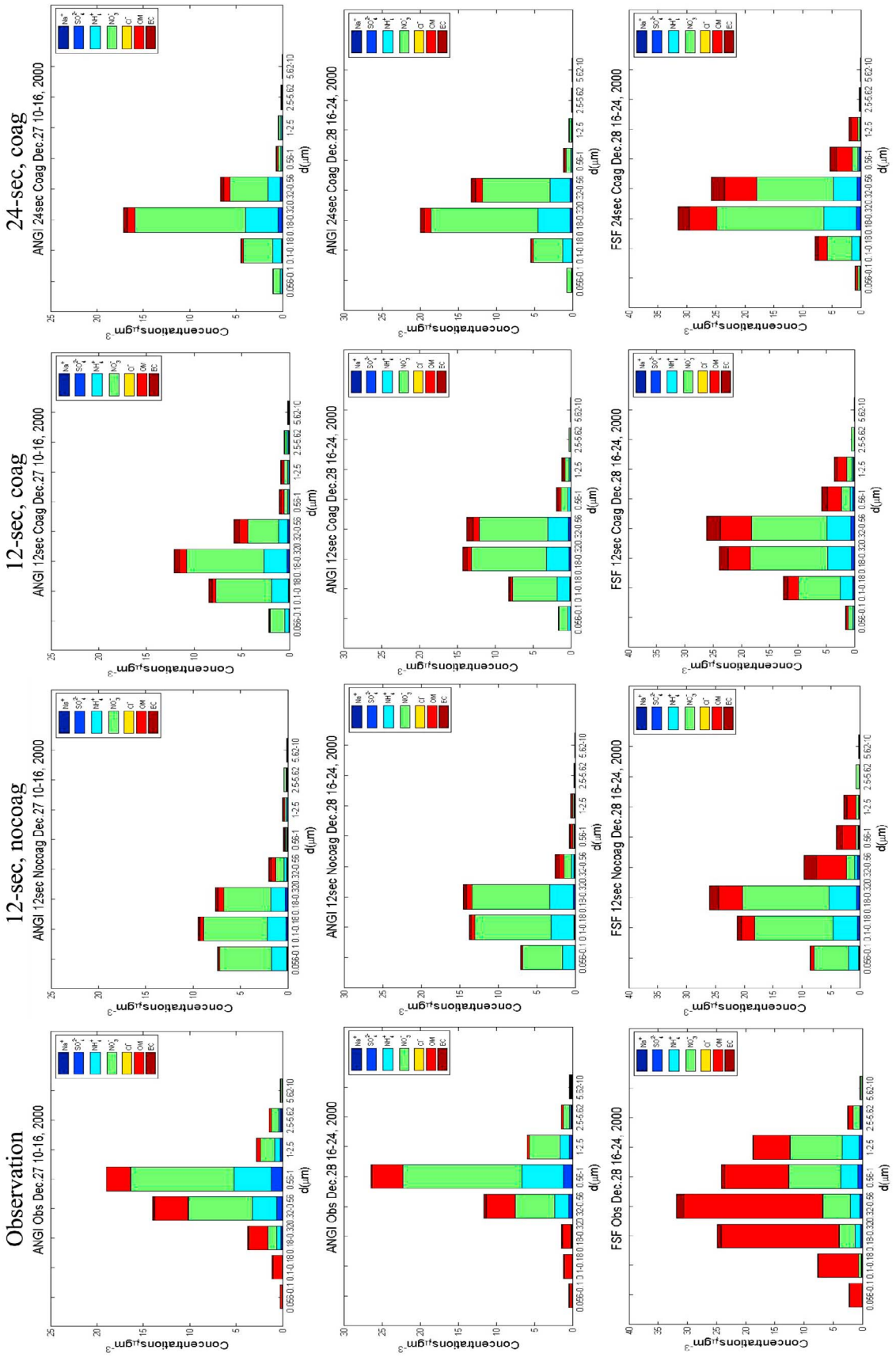

Figure 8. Observed and simulated particle size distributions during 10–16 Pacific Standard Time (PST) on 27 December 2000 at ANGI and during 16–24 PST on 28 December 2000 at ANGI and FSF. The simulation results are from the 12 sec simulations without and with coagulation (12 sec, nocoag and 12 sec, coag, respectively) and the 24 sec simulation with coagulation (24 sec, coag).

3.3. Evaluation of Size Distribution and Number Concentrations of $PM_{2.5}$

[15] Figure 8 compares the simulated particle size distributions with eight stage MOUDI observations by Desert Research Institute (DRI) during 10–16 PST (daytime) on 27 December at ANGI and during 16–24 PST (nighttime) on 28 December at ANGI and FSF. The observed $PM_{2.5}$ mass concentrations peaked in the diameter range of 0.56–1.0 μm on both days at ANGI and 0.32–0.56 μm at FSF, with the dominance of NH_4NO_3 at ANGI and both OM and NH_4NO_3 at FSF for $PM_{2.5}$. The smaller peak diameter at FSF reflects the abundance of freshly emitted smaller PM near the source as compared with that away from the source at ANGI at which ultrafine PM may have grown into larger size ranges through coagulation and condensation processes. Similar dominance of OM and NH_4NO_3 in observed size-resolved $PM_{1.8}$ mass concentrations at other sites such as Bakersfield, Modesto, and Sacramento during CRPAQS has also been reported by other studies [e.g., *Herner et al.*, 2005]. *Magliano et al.* [2005] also found that NH_4NO_3 and carbonaceous aerosols (i.e., EC and OC) account for >80% of $PM_{2.5}$ mass concentrations observed at urban and rural sites, with more NH_4NO_3 at rural sites than urban sites (63% versus 47%) and more carbonaceous particles at urban sites than rural sites (35% versus 17%) during winter episodes. These observed PM size distributions represent two distinct patterns in the SJV [*Herner et al.*, 2006] and other regions in the U.S. [e.g., *Zhang et al.*, 1993]: hygroscopic secondary PM composing primarily of NH_4^+, NO_3^-, and SO_4^{2-} at ANGI and less hygroscopic primary PM composing mostly of OM and EC at FSF. While the model also predicts the dominance of NH_4NO_3 at both ANGI and FSF, it fails to reproduce the extremely high concentrations of OM at FSF, indicating the underestimate in primary OM emissions from mobile sources during rush hours and residential wood combustion during evening hours at FSF. During 10–16 PST on 27 December at ANGI, the 12 sec simulation with coagulation predicts the peak concentration to be in the diameter range of 0.18–0.32 μm, which is closer to the observed peak concentration size range of 0.56–1 μm than that without coagulation (i.e., 0.1–0.18 μm). Compared with the 12 sec simulation with coagulation, the use of 24 sections gives the peak mass concentration and the concentrations in the first two size sections ($\leq$0.18 μm) closer to the observations, although it significantly overpredicts the mass concentration in the diameter range of 0.18–0.32 μm and underpredicts that in the diameter range of 0.32–1.0 μm. The misalignment in the peak bin between observation and simulation indicates a slower simulated particle growth rate than observed. During 16–24 PST on 28 December at ANGI, compared with the 12 sec simulation without coagulation, the 12 sec simulation with coagulation allows a growth of PM into the size section of 0.32–0.56 μm from lower sections. Among all simulations, the 24 sec simulation gives a size distribution that is the closest to the observation in term of peak value and overall shape. During 16–24 PST on 28 December at FSF, the 12 sec simulation with coagulation gives the peak concentration in the same size range (i.e., 0.32–0.56 μm) as the observation. The 12 sec simulation without coagulation and the 24 sec simulation with coagulation predict the peak concentration in the size range of 0.18–0.32 μm but 24 sec simulation reproduces the peak mass concentration better than both 12 sec simulations. Overall, the model overpredicts the PM mass concentrations with diameters smaller than 0.32 μm and consequently underpredicts those in the larger size range (i.e., 0.32–2.5 μm at ANGI and 0.56–2.5 μm at FSF). The total mass concentrations of OM over the entire size range are underpredicted significantly at both sites, particularly at FSF, due to the underestimate in primary OM emissions. The total mass concentrations of NH_4^+ are overpredicted during 10–16 on 27 December at ANGI and during 16–24 PST on 28 December at FSF but underpredicted during 16–24 PST on 28 December at ANGI. The total mass concentrations of SO_4^{2-} are well reproduced at FSF but underpredicted at ANGI. The total mass concentrations of NO_3^- are slightly overpredicted at ANGI, which is more consistent with the trends for the 24 h average comparison (Figure not shown) than the significant overprediction trends in the hourly comparison (see Figure 7). They are, however, significantly overpredicted at FSF, which is fairly consistent with the trends of the 24 h average and hourly comparison shown in Figures 4 and 7, despite self-inconsistency in NO_3^- measurements in the three data sets used for model evaluation. The NO_3^- observations were obtained using different methods by different investigators during CRPAQS, e.g., the Minivol filter sampler for the 24 h average, the continuous NO_3^- analyzer for the hourly values, and the MOUDI sampler for the 5–8 h average size-resolved values. The 24-average NO_3^- concentrations on 27 December obtained or derived based on observations using the three methods are 23.4, 14.6, and 20.7 $\mu g\ m^{-3}$, respectively, at ANGI and 17.2, 12.8, and 33.9 $\mu g\ m^{-3}$ at FSF, indicating large uncertainties in NO_3^- measurements.

[16] The above results show that coagulation is an important process shaping the PM size distribution during this week-long episode. Other important processes include emissions, homogeneous nucleation, condensation/evaporation, removal, and transport; the inaccurate treatments for any of which in the model may contribute to the errors in the simulated PM size distribution. Several possible factors may help explain the discrepancies in observed and simulated size-resolved composition and size distribution shown in Figure 8, including the uncertainties in the emissions of primary OM and secondary inorganic PM precursors such as SO_2, NO_x, and NH_3, the inaccuracy in gas/particle partitioning of TNO3 and TNH4, the assumed initial size distribution of PM emissions and initial and boundary conditions, the high uptake coefficient of N_2O_5 used, the uncertainty in the homogeneous nucleation parameterization used, the insufficient growth by condensation due primarily to underestimate in condensable masses, and incapability of the full equilibrium gas/particle mass transfer approach in simulating coarse NO_3^-.

[17] Figure 9 shows the spatial distributions of the simulated weekly mean mass and number concentrations of $PM_{0.001\_0.01}$, $PM_{0.01\_0.1}$, $PM_{0.1\_1}$, $PM_{1\_2.5}$, $PM_{2.5}$, and $PM_{10\_2.5}$ from the 12 sec simulation with and without coagulation. The mass concentrations of $PM_{0.01\_0.1}$, $PM_{0.1\_1}$, $PM_{1\_2.5}$, and $PM_{10\_2.5}$ peak in the SJV and over the oceanic area, whereas those of $PM_{0.001\_0.01}$ peak in the remaining areas, leading to similar variations in their number concentrations from the simulation without coagulation. In the northwestern portion of Nevada (e.g., Washoe, Carson City, Douglas, Lyon, Storey, and Churchill counties), the emissions of CO, SO_2, VOCs, and PM_{10}, from several sources including residential wood smoke

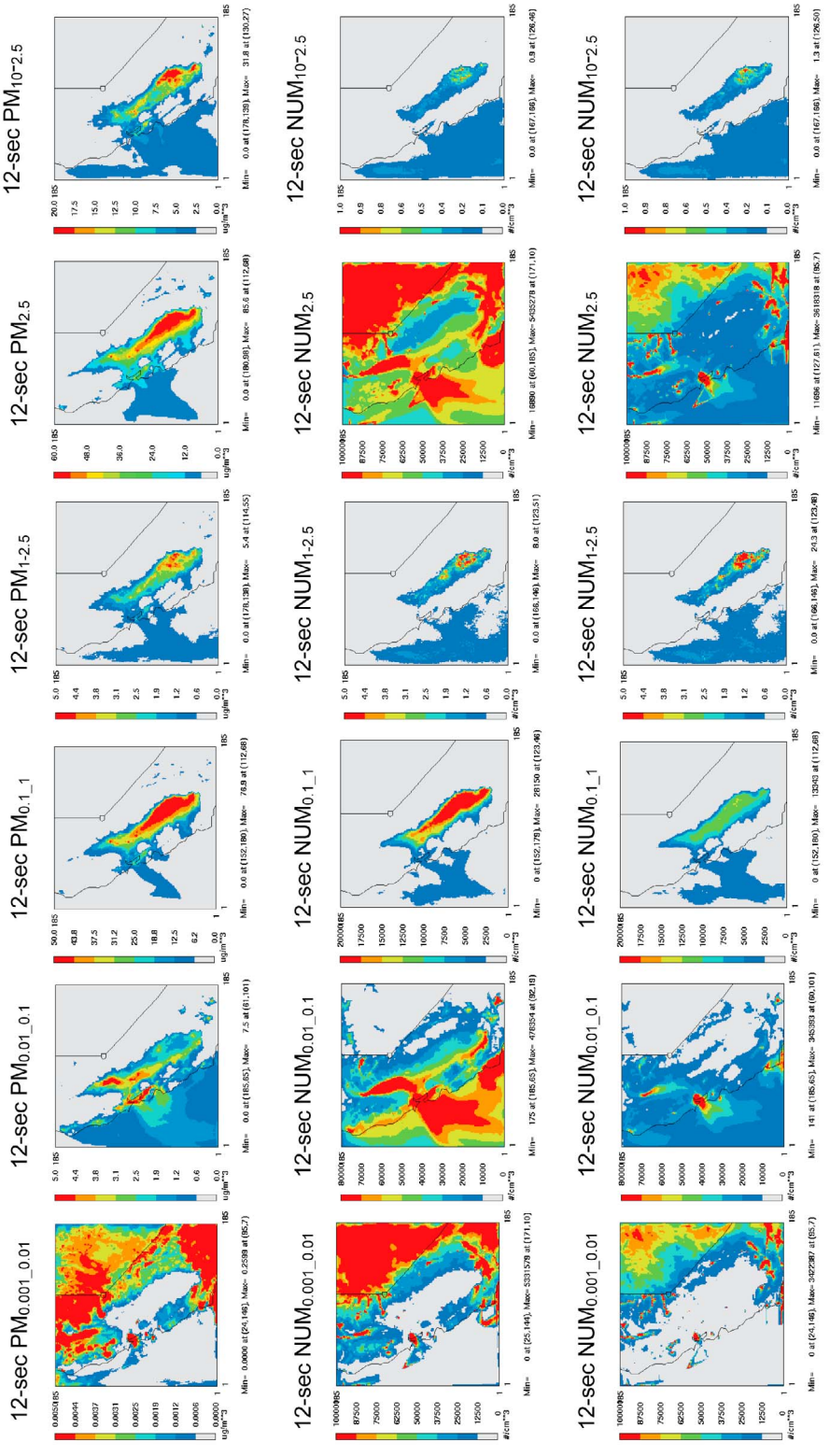

Figure 9. Simulated spatial distributions of weekly mean mass and number concentrations of $PM_{0.001\_0.01}$, $PM_{0.01\_0.1}$, $PM_{0.1\_1}$, $PM_{1\_2.5}$, $PM_{2.5}$, and $PM_{10\_2.5}$ from the 12 sec simulations without (row 2) and with (rows 1 and 3) coagulation.

and other mobile, point, and industrial sources peak in winter seasons, when winds are relatively calm during nighttime and early morning, leading to the highest pollutant concentrations of SO_4^{2-}, EC, and OM in the size range of 0.001–0.01 μm in this region as well as a relatively large amount of new particles formed via homogeneous nucleation. In the SJV, higher $PM_{0.01\_0.1}$ concentrations occur in the northern portion because of the relative abundance of ultrafine carbonaceous aerosols (i.e., EC and OM). The mass concentrations of $PM_{0.1\_1}$ are high in the central and southern portions of the valley, and those of $PM_{1\_2.5}$ and $PM_{10\_2.5}$ are high in the southern portion, due to the dominance of NH_4NO_3 in the accumulation mode and nitrate salts such as $NaNO_3$ in the coarse mode. Treating coagulation process reduces the number concentrations of submicron PM (i.e., $PM_{0.001\_0.01}$, $PM_{0.01\_0.1}$, and $PM_{0.1\_1.0}$ effectively (by 30–100%, 30–88%, and 10–83%, respectively) but less effectively for those of PM with diameter greater than 1.0 μm. It is generally accepted that the coagulation process is too slow to affect $PM_{2.5}$ mass concentrations in 3-D model simulations [e.g., *Wexler et al.*, 1994]. However, coagulation may affect the number concentrations of fine and ultrafine particles and this study demonstrates the importance of coagulation for simulating PM number size distributions. As a result of the competition between sources (e.g., emissions and homogeneous nucleation) and growth/removal (e.g., coagulation and dry/wet deposition) processes, the number concentrations peak over land areas in the state of Nevada and the southeast of the SJV for $PM_{0.001\_0.01}$, the oceanic area and the northwest of the SJV for $PM_{0.1\_1}$, and the oceanic area and the SJV for $PM_{0.01\_0.1}$, $PM_{1\_2.5}$, and $PM_{10\_2.5}$. For example, $PM_{0.001\_0.01}$ dominates the number concentrations over land areas in Nevada and the southeast of the SJV, which may be due to the slower growth rates of emitted or formed ultrafine particles in this region as a result of the lower water vapor (thus humidity), as compared with ultrafine particles emitted/formed in the western portion of the domain where the humidity is much higher. The resulting number concentrations of $PM_{2.5}$ with the coagulation process are in the range of ~10,000 to ~40,000 cm^{-3} over most of the SJV, and 11,696 to 3,618,318 cm^{-3} over the remaining land and oceanic areas. Note that the effects of coagulation on the number concentrations in the San Francisco (SF) Bay area and in an area in the northern domain that covers Glenn, Colusa, Butte, and Sutter countries are relatively small. This can be attributed to two main causes. First, SO_2 emissions in the SF Bay area are the highest in the simulation domain (figure not shown), resulting in the highest H_2SO_4 and SO_4^{2-} concentrations in the domain (see Figure 3b). The abundance of H_2SO_4 and water vapor available in this area leads to a faster new particle formation rate via homogeneous nucleation than in other areas, which effectively replenishes some losses of particle numbers due to coagulation. Second, in both the SF Bay area and the northern domain, the emissions of primary PM species such as BC, OM, NO_3^-, and SO_4^{2-} in the size range of <0.1 μm are among the highest, which could also serve as a source to compensate for the loss in PM number concentrations due to coagulation.

[18] Figure 10 shows the simulated and observed number concentrations for the eight size stages between 0.056 and 10 μm at ANGI and FSF averaged for the sampling time windows during five sampling periods on 26–28 December 2000. At ANGI, compared with the simulations without coagulation, the simulations with coagulation give lower number concentrations of $PM_{0.056\_0.1}$ and $PM_{0.1\_0.18}$, improving model performance in both bins during 10–16 27 December and 16–24 28 December and in the size range of 0.1–0.18 mm during other sampling periods. Such simulations give higher number concentrations of $PM_{0.32\_0.56}$, $PM_{0.56\_1.0}$, and $PM_{1.0\_2.5}$ during the five sampling periods, decreasing the underpredictions in the number concentrations for those size sections except during 5–10 A.M. on 26 December. The underpredictions in simulated number concentrations from the simulations with coagulation are due likely to the underestimate in primary PM emissions and new particle formation rates from homogeneous nucleation of H_2SO_4 and H_2O. At FSF, the coagulation process reduces overpredictions in the number concentrations of PM with diameter less than 0.32 μm during 10–16 PST on 27 December, between 0.1 and 0.32 μm during 5–10 PST on 26 and 28 December, and during 16–24 PST on 28 December, although it increases underpredictions between 0.056 and 0.1 μm during all sampling periods except for 10–16 PST on 27 December. At both sites, the 12 and 24 sec simulations with coagulation generally give similar number concentrations, although differences exist for some size ranges, in particular, between 0.32 and 0.56 μm during most sampling periods and between 0.56 and 2.5 μm during some periods (e.g., 5–10 PST on 26 December and 5–10 PST on 28 December at ANGI). This is due mainly to the difference in the coagulation growth rates and dry deposition rates simulated between the 12 and 24 sec size structures. Table 2 summarizes the performance statistics for PM number concentrations over the eight size stages. The observed average $PM_{5.62}$ number concentrations at ANGI and FSF during the five sampling time periods are 22694.4 cm^{-3} (with a range of 5566–29455 cm^{-3} and an average of 17929 cm^{-3} at ANGI and a range of 10,534–43,231 cm^{-3} and an average of 26,660 cm^{-3} at FSF). For comparison, the observed hourly average PM_{10} number concentrations at FSF during 15 December 2000 to 3 February 2001 range from 2700 to 89,000 cm^{-3}, with an average of 22,000 cm^{-3} at FSF (obtained using a PM_{10} inlet with a TSI Scanning Mobility Particle Sizer (SMPS) (0.009–0.392 μm diameter in 52 channels) and a PMS Lasair (LAS) 1003 optical particle counter (0.1–2 μm in seven channels)) [*Watson et al.*, 2002]. Both 12 and 24 sec simulations with coagulation reduce the overpredictions at both sites, changing the NMB of 118.5% to −21.8% for the 12 sec simulation and the NMB of 147.1% to –13.9% for the 24 sec simulation; they also increase the correlation coefficient (R) from 0.07 to 0.46, indicating an overall improvement in the PM number concentration predictions.

4. Summary

[19] CMAQ-MADRID 1 with 12 and 24 size section simulations are conducted to simulate aerosol mass, number, and size distributions in central CA during 25–31 December 2000. Both 12 and 24 sec simulations reproduce well the high mass concentrations of $PM_{2.5}$ in the Central Valley, but large biases exist in simulated mass concentrations of PM components, particularly in OM, NO_3^-, and EC. While NO_3^- and NH_4^+, two major $PM_{2.5}$ components in this area, are overpredicted by 32.1%–40.2% and 18.7%–23.6%, respectively,

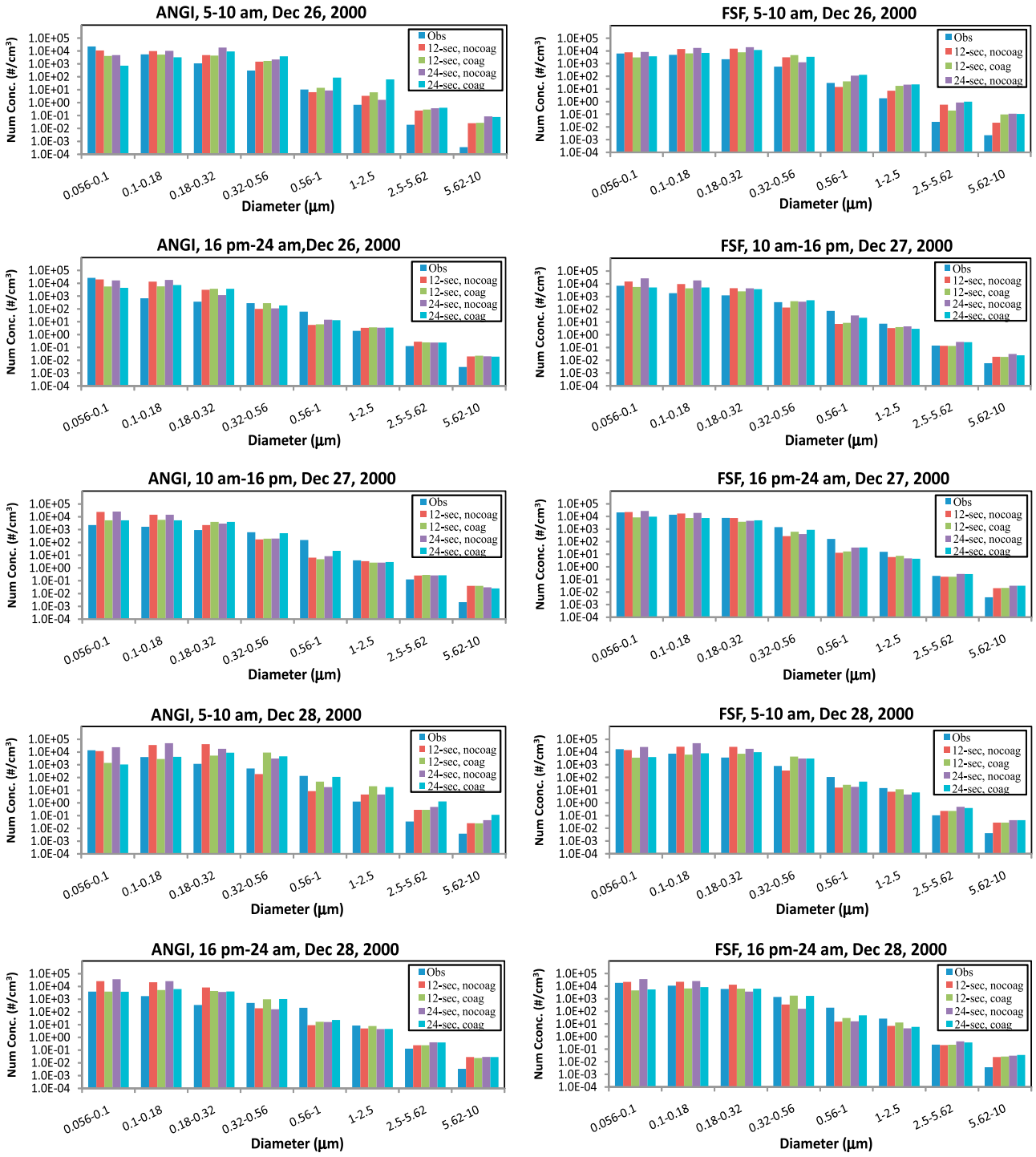

Figure 10. Observed and simulated PM number concentrations in the eight size stages at (a) ANGI (left) and (b) FSF (right) during five sampling periods on 26–28 December 2000. The observations are derived based on the MOUDI size-resolved mass concentrations over the eight stages and the simulation results are from the 12 and 24 sec simulations without and with coagulation.

OM is underpredicted by 67% and EC is overpredicted by 36%–37%. Several factors may contribute to model biases, including the underestimates in the emissions of primary OM and secondary PM precursors such as NH_3, SO_2, or NO_x; the uncertainties in the model treatments (e.g., the gas- and aqueous-phase chemistry, the heterogeneous chemistry of N_2O_5, the gas/particle partitioning of TNO3 and TNH4); and inaccuracy in simulated meteorological variables (e.g., solar radiation, temperature, RH, mixing height, and cloud fractions). While the 12 and 24 sec simulations reproduce well the magnitudes of the 24 h average $PM_{2.5}$ mass concentrations, they fail to capture the temporal variations of $PM_{2.5}$ at nearly all the sites. Inaccuracies in precursor emissions, model difficulties in simulating meteorology over complex terrain

Table A1. List of CRPAQS Sites Included in the Model Evaluation[a]

No.	Site Code	Site Name	Site Coordinates (Lat, Lon)	Elevation (msl, m)	No.	Site Code	Site Name	Site Coordinates (Lat, Lon)	Elevation (msl, m)
1	ACP	Angels Camp	(38.0058, −120.0014)	373	29	KCW	Kettleman City	(36.0947,−119.9475)	103
2	ALT1	Altamont Pass	(37.7175,−121.6603)	350	30	KRV	Sierra Nevada Foothills-Kings River Valley	(36.9022, −119.3058)	509
3	ANGI	Angiola	(35.9481,−119.5378)	60	31	LVF	Livermore Old 1st St.	(37.685, −121.766)	146
4	BAC	Bakersfield California Ave.	(35.3567,−119.0625)	119	32	LVR1	Rincon St., Livermore	(37.6875,−121.7842)	138
5	BARS	Barstow	(34.9786,−117.1856)	648	33	M14	Modesto (14th St.)	(37.6419,−120.9944)	28
6	BGS	Bakersfield Stn	(35.3858, −119.0117)	126	34	MOP	Mojave (Poole St.)	(35.0506, −118.1483)	832
7	BODB	Bodega Bay Stn	(38.3189,−123.0728)	17	35	MRM	Merced-Midtown	(37.3083,−120.4806)	53
8	BQUC	Bouquet Canyon	(34.805, −118.7203)	1004	36	OLD	Oildale (Manor)	(35.4381,−119.0169)	180
9	BRES	BAC residential area	(35.3581, −119.0836)	117	37	OLW	Olancha	(36.2678, −117.9928)	1124
10	BTI	Bethel Island Stn	(38.0064, −121.6419)	2.0	38	ORE	Corcoran	(36.0875,−119.5658)	62
11	CAJP	Cajon Pass	(34.3686, −117.4478)	1277	39	PAC1	Pacheco Pass	(37.0733,−121.2217)	452
12	CANT	Cantil	(35.3069, −117.9694)	613	40	PATT	Patterson Pass	(40.295,−122.8667)	1067
13	CARP	Carrizo Plain	(35.3142, −119.9958)	598	41	PIXL	Pixley National Wildlife Refuge	(35.9136,−119.3758)	69
14	CHL	China Lake	(39.7303, −121.844)	61	42	PLE	Pleasant Grove	(37.7,−121.91)	99
15	CLO	Clovis Stn	(36.8194,−119.7164)	108	43	S13	Sacramento (T St.)	(38.5683,−121.4933)	6
16	COP	Corcoran-Patterson Ave.	(36.1022, −119.5658)	63	44	SDP	Sacramento Stn (Del Paso Manor)	(38.6136,−121.3681)	26
17	DUB1	Dublin	(37.695, −121.9689)	250	45	SELM	Selma Airport	(36.5828, −119.6603)	94
18	EDI	Edison	(35.3503, −118.9572)	118	46	SFA	San Francisco (Arkansas St.)	(37.7658,−122.3989)	6
19	EDW	Edwards Air Force Base	(34.9294, −117.9042)	724	47	SJ4	San Jose (4th St.)	(37.3397,−121.8886)	26
20	FEDL	Dairy	(36.6111, −119.8553)	76	48	SNFH	Sierra Nevada Foothills Stn	(37.0625,−119.4961)	589
21	FEL	Fellows	(35.2025,−119.5458)	359	49	SOH	Stockton Stn (Hazelton St.)	(37.9503,−121.2689)	8
22	FELF	Foothills above FEL	(35.1706,−119.5569)	512	50	SWC	SW Chowchilla	(37.0481, −120.4717)	43
23	FREM	Fresno area near Hwy 41	(36.78, −119.7833)	96	51	TEH2	Tehachapi Pass	(25.1678,−118.4819)	1229
24	FRES	FSF residential area	(36.7831,−119.7683)	96	52	TEJ	Tejon Pass	(34.8869,−118.9142)	946
25	FSD	Fresno (Drummond)	(36.7056, −119.7414)	91	53	VCS	Visalia (Church St.)	(36.3325,−119.2911)	102
26	FSF	Fresno (First St.)	(36.7817,−119.7733)	97	54	WAG	Walnut Grove Tower Stn	(38.2644,−121.4906)	3
27	HAN	Hanford (Irwin St.)	(36.3147,−119.6439)	76	55	YOD	Yoder St.	(36.1018,−119.5584)	64
28	HELM	Helm-Central Fresno County	(36.5906, −120.1772)	55	56	YOSE	Yosemite National Park	(37.7114,−119.6958)	1685

[a]Compiled based on http://www.arb.ca.gov/airways/crpaqs/siteAtlas/siteatlas.htm and CARB data collections. All sites are satellite sites except 3 year-round anchor sites (ANGI, BAC, and FSF) and five winter anchor sites (BTI, SDP, SJ4, SNFH, and WAG).

Table A2. List of the "Backbone" Network of CARB and Air Pollution Control District Sites Included in the Model Evaluation[a]

No.	Site Code	Site Name	Site Coordinates (Lat, Lon)	Elevation (msl, m)	No.	Site Code	Site Name	Site Coordinates (Lat, Lon)	Elevation (msl, m)
1	ARV	Arvin Stn	(35.2083, −118.784)	145	37	PGV	Pleasant Grove Stn (4 SW)	(38.7669,−121.514)	50
2	ATL	Atascadero (Lewis Ave.)	(35.4917,−120.668)	262	38	PIRU	Piru Stn (Pacific Ave.)	(34.4046,−118.8251)	0
3	BSW	Barstow Stn	(34.8939,−117.023)	692	39	PLR	Parlier Stn	(36.6,−119.508)	166
4	CA1	Capitan Stn/Las Flores Canyon #1	(34.4897,−120.0458)	0	40	PRF	Paso Robles Stn (Santa Fe)	(35.6317,−120.69)	100
5	CCD	Concord Stn (Treat Blvd.)	(37.9386,−122.025)	26	41	RED	Redwood City Stn	(37.4811,−122.203)	5
6	CHM	Chico Stn (Manzanita)	(39.7564,−121.847)	61	42	ROC	Rocklin Stn (Rocklin Rd.)	(38.7889,−121.217)	100
7	CRP	Corcoran Stn (Van Dorsten)	(34.4047,−119.456)	152	43	ROS	Roseville Stn (N Sunrise)	(38.7458,−121.265)	161
8	CSS	Colusa Stn (Sunrise Blvd.)	(39.2028,−122.017)	17	44	SALH	Salinas Stn (High School)	(36.6944,−121.6222)	33
9	DVP	Davenport Stn	(37.0043,−122.114)	0	45	SCFS	Santa Clarita Stn (County Fire Stn)	(34.3875,−118.5336)	375
10	DVS	Davis/UCD Campus Stn	(38.5333, −121.775)	16	46	SFA	San Francisco Stn(Arkansas St.)	(37.7658, −122.3989)	6
11	ECHO	Echo Summit Stn (HWY 50)	(38.8116,−120.0324)	2250	47	SFEL	San Francisco Stn (Ellis St.)	(37.7841,−122.431)	70
12	ECP	El Capitan Beach Stn	(34.4608,−120.027)	30	48	SGS	San Andreas Stn (Gold Strike Rd.)	(38.2,−120.667)	307
13	EDS	Edison Stn	(35.3461,−118.851)	128	49	SHA	Shafter Stn (Walker St.)	(35.5,−119.268)	126
14	ELK	Elk Grove Stn (Bruceville Rd.)	(38.3019,−121.422)	6	50	SLM	San Luis Obispo Stn (Marsh)	(35.2839,−120.654)	66
15	FCW	Fremont Stn (Chapel Way)	(37.5356,−121.961)	18	51	SMAR	Santa Maria Stn (S Broadway)	(34.9498,−120.434)	76
16	FLN	Folsom Stn (Natoma St.)	(38.6839,−121.1627)	0	52	SNB	Sonora Stn (S Barretta St.)	(37.9817,−120.379)	0
17	FSS	Fresno Stn (Sierra Skypark #2)	(36.8417,−119.874)	98	53	SNH	Sacramento-North Highlands Stn (Blackfoot Way)	(38.7122,−121.381)	8
18	GCL	Grover City Stn (Lesage Dr.)	(35.125,−120.633)	4	54	SOC	Stockton Stn (Claremont)	(37.9945,−121.3078)	13
19	GNF	Goleta Stn (N Fairview Ave.)	(34.4452,−119.8166)	50	55	SPEP	San Pablo Stn (El Portal)	(37.9643,−122.3391)	15
20	GVB	Gaviota TC-Site B Stn	(34.5275,−120.196)	305	56	SRF	Santa Rosa Stn (Fifth St.)	(38.4453,−122.708)	49
21	JAC	Jackson Stn (Clinton Rd.)	(38.34,−120.763)	377	57	SRL	San Rafael Stn	(37.9728,−122.5184)	11
22	LHS	Lompoc Stn (HS & P)	(34.7247,−120.428)	244	58	SYN	Santa Ynez Airport Stn	(34.6028,−120.071)	204
23	LMK	Mineral King Lookout Pt. Stn	(36.4292,−118.7625)	0	59	TEF	Nipomo Stn (Teft and Pomeroy St.)	(35.0283,−120.3872)	101
24	LOM	Lompoc Stn (AWOS)	(34.6375,−120.456)	24	60	TPP	Tracy Stn (Patterson Pass)	(37.7381,−121.5345)	31
25	LPD	Los Padres NF Stn (Paradise Rd.)	(34.5403,−119,789)	547	61	TRON	Trona Stn (Athol and Telegraph)	(35.7638,−117.3961)	545
26	LTY	South Lake Tahoe Stn (Sandy)	(38.945,−119.969)	0	62	TSM	Turlock Stn (S Minaret)	(36.4886,−120.835)	56
27	LWP	Lancaster Stn (W. Pondera St.)	(34.6903,−118.128)	725	63	UKG	Ukiah Stn (E Gobbi Street)	(39.1447,−123.2065)	194
28	M29	Madera Stn (29 1/2 No. of Ave 8)	(36.8667,−120.01)	0	64	VBS	Vandenberg STS Power Plant Stn	(34.5947,−120.636)	100
29	MAG	Mammoth Lakes/Gateway HC Stn	(37.6333,−118.967)	2396	65	VICT	Victorville Stn (Park Ave.)	(34.51,−117.3305)	913
30	MRA	Merced Stn (S Coffee Ave.)	(37.2825,−120.433)	86	66	VJO	Vallejo Stn (Tuolumne St.)	(38.1042,−122.235)	23
31	NAP	Napa Stn (Jefferson Ave.)	(38.25,−122.3)	6	67	VIA	Victorville/Armagosa Stn	(34.0625,−117.319)	876
32	NAT	Sacramento/Natoma (Airport Rd.)	(38.6369,−121.513)	5	68	VTA	Ventura Co./W Casitas Pass Stn	(34.3869, −119.416)	319
33	OJO	Ojai Stn (Ojai Rd.)	(34.4167,−119,2458)	262	69	WCM	White Cloud Mtn. Stn	(39.3166,−120.8444)	1302
34	OKA	Oakland Stn (Alice St.)	(37.8014,−122.2672)	7	70	WLM	Willits Stn (S Main St.)	(39.403,−123.3491)	420
35	PBG	Pittsburg Stn (10th St.)	(38.0296,−121.8969)	9	71	WLW	Willows Stn (E Laurel St.)	(39.5208,−121.2082)	41
36	PGN	Placerville Stn (Gold Nugget)	(38.7272,−120,818)	0	72	YAS	Yuba City Stn (Almond St.)	(39.1389,−121.618)	20

[a]Compiled based on *Watson et al.* [1998], http://www.sonomatechdata.com/crpaqsmetrep/sites.cfm, and CARB data collection.

during a strong stagnation event (e.g., inability of meteorological schemes in capturing local scale variations), and uncertainties in model formulation (e.g., aerosol formation and removal processes) may contribute to the difference between simulated and observed temporal variations of $PM_{2.5}$. In addition, inconsistencies and uncertainties in observations with different methods introduce added complexity in an accurate assessment of model's capability in simulating mass concentrations of $PM_{2.5}$ and its components.

[20] Although all simulations overpredict the mass concentrations of PM with diameter smaller than 0.32 μm and underpredict those in the size range of 0.32–5.62 μm, the 24 sec simulation with coagulation produces a PM size distribution with peak concentrations and overall shapes that are the closest to the observations among all simulations. Sensitivity simulation results show that the coagulation process leads to 40%–91% reduction of simulated $PM_{2.5}$ number concentrations and an overall closer agreement with observed PM number concentrations than those without coagulation. The NMB of the simulated $PM_{5.62}$ number concentrations changes from 118.5% to −21.8% for the 12 sec simulation and from 147.1% to −13.9% for the 24 sec simulation when the coagulation process is treated. These results indicate the importance of coagulation treatment for predicting particle number concentrations and the merits of using a fine size resolution in accurately simulating PM size distribution when computer resources are available. Several factors leading to the discrepancies in observed and simulated PM size distribution and number concentrations include the uncertainties in model inputs (e.g., the emissions of primary PM and PM precursors and the assumed initial size distribution of PM emissions) and formulation (e.g., heterogeneous chemistry, homogeneous nucleation, condensation, and gas/particle partitioning). While the coagulation process plays an important role, an accurate representation of other atmospheric processes in 3-D atmospheric models is necessary to reproduce the observed PM number concentrations and size distribution.

[21] Similar to many other modeling studies, some uncertainties exist in the model inputs and formulations as well as in the observational data set used for model performance evaluation in this study. Likely causes of discrepancies between simulations and observations as well as associated uncertainties identified in this work warrant additional diagnostic, sensitivity, and uncertainty studies for more quantitative estimates of sources of errors in the future. Given such uncertainties, accurately simulating $PM_{2.5}$ number and size distributions continues to be a major challenge in PM modeling in central CA and worldwide.

Appendix A

[22] Tables A1 and A2.

[23] **Acknowledgments.** This work was supported by San Joaquin Valleywide Study Agency (SJVSA) agreement 2004-03PM of the California Air Resources Board (CARB) through subcontract 2004-0378-5-24-04 from AER, Inc., and the NSF Career Award Atm-0348819 at NCSU. Thanks are due to the project manager Ajith Kaduwela, CARB, for his continuous support throughout this project and Greg O'Brien, Karen Magliano, Paul Livingstone, and Kemal Gurer, CARB, for providing observational data used in the model evaluation and valuable information regarding meteorological fields and emissions used in the model simulations. Thanks are also due to Judy Chow and Douglas Lowenthal, Desert Research Institute, for providing DRI's raw MOUDI measurement data for model evaluation and insightful discussions regarding these data.

References

Becker, S., J. M. Soukup, C. Sioutas, and F. R. Cassee (2003), Response of human alveolar macrophages to ultrafine, fine, and coarse urban air pollution particles, *Exp. Lung Res.*, *29*(1), 29–44, doi:10.1080/01902140303762.

Bhave, P., G. Sarwar, W. Appel, and R. Dennis (2006), Revised Treatment of N_2O_5 Hydrolysis in CMAQ, oral presentation at the 5th Annual CMAS Conference, Chapel Hill, N. C., October 16–18.

Blanco-Canqui, H., R. Lal, W. M. Post, R. C. Izaurralde, and M. J. Shipitalo (2006), Organic carbon influences on soil particle density and rheological properties, *Soil Sci. Soc. Am. J.*, *70*, 1407–1414, doi:10.2136/sssaj2005.0355.

Byun, D. W., and K. L. Schere (2006), Review of the governing equations, computational algorithms, and other components of the models-3 Community Multiscale Air Quality (CMAQ) Modeling System, *Appl. Mech. Rev.*, *59*, 51–77, doi:10.1115/1.2128636.

Chow, J. C., J. G. Watson, D. H. Lowenthal, P. A. Solomon, K. L. Magliano, S. D. Ziman, and L. W. Richards (1993), PM_{10} and $PM_{2.5}$ compositions in California's San Joaquin Valley, *Aerosol Sci. Technol.*, *18*, 105–128, doi:10.1080/02786829308959588.

Chow, J. C., J. G. Watson, D. H. Lowenthal, R. Hackney, K. L. Magliano, D. Lehrman, and T. Smith (1999), Temporal variations of $PM_{2.5}$, PM_{10}, and gaseous precursors during the 1995 Integrated Monitoring Study in central California, *J. Air Waste Manage. Assoc.*, *49*(PM), PM16–PM24.

Chow, J. C., L.-W. A. Chen, J. G. Watson, and D. H. Lowenthal (2006), $PM_{2.5}$ chemical composition and spatiotemporal variability during the California Regional $PM_{10}/PM_{2.5}$ Air Quality Study (CRPAQS), *J. Geophys. Res.*, *111*(D10), D10S04, doi:10.1029/2005JD006457.

Chow, J. C., J. G. Watson, D. H. Lowenthal, and K. L. Magliano (2008), Size-resolved aerosol chemical concentrations at rural and urban sites in Central California, USA, *Atmos. Res.*, *90*, 243–252, doi:10.1016/j.atmosres.2008.03.017.

Dabdub, D., L. L. DeHaan, and J. H. Seinfeld (1999), Analysis of ozone in the San Joaquin Valley of California, *Atmos. Environ.*, *33*(16), 2501–2514, doi:10.1016/S1352-2310(98)00256-8.

DaMassa, J., S. Tanrikulu, K. Magliano, A. J. Ranzieri, and E. Niccum (1996), Performance evaluation of SAQM in central California and attainment demonstration for the 3–6 August 1990 ozone episode, California Air Resources Board, Sacramento.

Davis, J. M., P. V. Bhave, and K. M. Foley (2008), Parameterization of N_2O_5 reaction probabilities on the surface of particles containing ammonium, sulfate, and nitrate, *Atmos. Chem. Phys.*, *8*, 5295–5311, doi:10.5194/acp-8-5295-2008.

Evans, M. J., and D. J. Jacob (2005), Impact of new laboratory studies of N_2O_5 hydrolysis on global model budgets of tropospheric nitrogen oxides, ozone and OH, *Geophys. Res. Lett.*, *32*(9), L09813, doi:10.1029/2005GL022469.

Ferreria, S. R. and E. M. Shipp (2005), Historical Meteorological Analysis in Support of the 2003 San Joaquin Valley PM10 State Implementation Plan, final report to CARB, prepared by San Joaquin Valley Air Pollution Control District, CA, Jan. 24.

Gilliland, A. B., K. W. Appel, R. W. Pinder, and R. L. Dennis (2006), Seasonal NH_3 emissions for the continental United States: Inverse model estimation and evaluation, *Atmos. Environ.*, *40*, 4986–4998, doi:10.1016/j.atmosenv.2005.12.066.

Harley, R., A. G. Russell, G. J. McRae, G. R. Cass, and J. H. Seinfeld (1993), Photochemical modeling of the Southern California Air Quality Study, *Environ. Sci. Technol.*, *27*, 378–388, doi:10.1021/es00039a019.

Harley, R., R. F. Sawyer, and J. B. Milford (1997), Updated photochemical modeling for California South Coast Air Basin: Comparison of chemical mechanisms and motor vehicle emission inventories, *Environ. Sci. Technol.*, *31*, 2829–2839, doi:10.1021/es9700562.

Held, T., Q. Ying, A. Kaduwela, and M. Kleeman (2004), Modeling particulate matter in the San Joaquin Valley with a source-oriented externally mixed three-dimensional photochemical grid model, *Atmos. Environ.*, *38*(22), 3689–3711, doi:10.1016/j.atmosenv.2004.02.053.

Helmig, D., L. Klinger, A. Guenther, L. Vierling, P. Zimmerman, and C. Geron (1999), Biogenic volatile organic compound emissions (BVOCs) I. Identifications from three continental sites in the U.S, *Chemosphere*, *38*, 2163–2187, doi:10.1016/S0045-6535(98)00425-1.

Herner, J. D., J. Aw, O. Gao, D. P. Chang, and M. J. Kleeman (2005), Size and composition distribution of airborne particulate matter in Northern California: 1. Particulate mass, carbon, and water soluble ions, *J. Air Waste Manage. Assoc.*, *55*, 30–51.

Herner, J. D., Q. Ying, J. Aw, O. Gao, D. P. Chang, and M. J. Kleeman (2006), Domain mechanisms that shape the airborne particle size and composition distribution in central California, *Aerosol Sci. Technol.*, *40*, 827–844, doi:10.1080/02786820600728668.

Ibald-Mulli, A., H. E. Wichmann, W. Kreyling, and A. Peters (2002), Epidemiological Evidence on Health Effects of Ultrafine Particles, *J. Aerosol Med.-Dep. Clear. Effects Lung*, *15*(2), 189–201.

Jacobson, M. Z. (1997), Development and application of a new air pollution modeling system–II. Aerosol module structure and design, *Atmos. Environ.*, *31*, 131–144, doi:10.1016/1352-2310(96)00202-6.

Jacobson, M. Z. (2001), GATOR-GCMM - 2. A study of daytime and nighttime ozone layers aloft, ozone in national parks, and weather during the SARMAP field campaign, *J. Geophys. Res.*, *106*(D6), 5403–5420, doi:10.1029/2000JD900559.

Jacobson, M. Z., R. P. Turco, E. J. Jensen, and O. B. Toon (1994), Modeling coagulation among particles of different composition and size, *Atmos. Environ.*, *28A*, 1327–1338, doi:10.1016/1352-2310(94)90280-1.

Jacobson, M. Z., Y. J. Kaufmann, and Y. Rudich (2007), Examining feedbacks of aerosols to urban climate with a model that treats 3-D clouds with aerosol inclusions, *J. Geophys. Res.*, *112*(D24), D24205, doi:10.1029/2007JD008922.

Jin, L., S. Tonse, D. S. Cohan, X. L. Mao, R. A. Harley, and N. J. Brown (2008), Sensitivity analysis of ozone formation and transport for a central California air pollution episode, *Environ. Sci. Technol.*, *42*, 3683–3689, doi:10.1021/es072069d.

Kleeman, M. J., Q. Ying, and A. Kaduwela (2005), Control strategies for the reduction of airborne particulate nitrate in California's San Joaquin Valley, *Atmos. Environ.*, *39*, 5325–5341, doi:10.1016/j.atmosenv.2005.05.044.

Kumar, N. K., F. W. Lurmann, and S. N. Pandis (1998), Analysis of Atmospheric Chemistry during 1995 Integrated Monitoring Study, Report No. STI-997214-1791-DFR, Prepared for California Air Resources Board, Sacramento, CA, by Sonoma Technology Inc., Santa Rosa, CA.

Liang, J., A. Kaduwela, B. Jackson, K. Gurer, and P. Allen (2006), Off-line diagnostic analysis of a three-dimensional PM model using two matrix factorization methods, *Atmos. Environ.*, *40*, 5759–5767, doi:10.1016/j.atmosenv.2006.05.035.

Livingstone, P. L., et al. (2009), Simulating PM concentration during a winter episode in a subtropical valley: Sensitivity simulations and evaluation methods, *Atmos. Environ.*, doi:10.1016/j.atmosenv.2009.07.033.

Lu, C.-H., and J. S. Chang (1998), On the indicator-based approach to assess ozone sensitivities and emissions features, *J. Geophys. Res.*, *103*(D3), 3453–3462, doi:10.1029/97JD03128.

Lurmann, F. W., A. S. Wexler, S. N. Pandis, S. Musarra, N. Kumar, and J. H. Seinfeld (1997), Modeling urban and regional aerosols: II. Application to California's south coast air basin, *Atmos. Environ.*, *31*, 2695–2715, doi:10.1016/S1352-2310(97)00100-3.

MacDonald, C. P., M. C. McCarthy, T. S. Dye, N. J. M. Wheeler, H. R. Hafner, and P. T. Roberts (2003), Transport and dispersion during wintertime particulate matter episodes in the San Joaquin Valley, California, *J. Air Waste Manage. Assoc.*, *56*, 961–976.

Magliano, K. L., V. M. Hughes, L. R. Chinkin, D. L. Coe, T. L. Haste, N. Kumar, and F. W. Lurmann (1999), Spatial and temporal variations in PM_{10} and $PM_{2.5}$ source contributions and comparison to emissions during the 1995 Integrated Monitoring Study, *Atmos. Environ.*, *33*(29), 4757–4773, doi:10.1016/S1352-2310(99)00265-4.

Magliano, K., T. Najita, and K. Turkiewicz (2005), Comparison of air quality during two winter episodes, American Association for Aerosol Research (AAAR), Supersites Conference, February, Atlanta, GA.

McCarthy, M., S. Brown, F. Lurmann, and P. Roberts (2005), The role of nighttime chemistry in winter ammonium nitrate formation in the San Joaquin Valley, American Association for Aerosol Research (AAAR), Supersites Conference, February, Atlanta, GA.

Neuman, J. A., et al. (2003), Variability in ammonium nitrate formation and nitric acid depletion with altitude and location over California, *J. Geophys. Res.*, *108*(D17), 4557, doi:10.1029/2003JD003616.

Oberdörster, G. (1996), Significance of particle parameters in the evaluation of exposure-dose relationships of inhaled particles, *Inhal. Toxicol.*, *8*, Suppl., 73–90.

Pun, B., and C. Seigneur (1999), Understanding particulate matter formation in the California San Joaquin Valley: Conceptual model and data needs, *Atmos. Environ.*, *33*, 4865–4875, doi:10.1016/S1352-2310(99)00266-6.

Pun, B., and C. Seigneur (2001), Sensitivity of particulate matter nitrate formation to precursor emissions in the California San Joaquin Valley, *Environ. Sci. Technol.*, *35*, 2979–2987, doi:10.1021/es0018973.

Pun, B. K., C. Seigneur, J. Pankow, E. Chang, R. Griffin, and E. Knipping (2005), An Upgraded Absorptive Secondary Organic Aerosol Partitioning Module for Three-dimensional Air Quality Applications, paper 7B4, the 24th Annual AAAR Conference, October 2005, Austin, TX.

Pun, B. K., C. Seigneur, K. Vijayaraghavan, S.-Y. Wu, S.-Y. Chen, E. M. Knipping, and N. Kumar (2006), Modeling regional haze in the BRAVO study using CMAQ-MADRID: 1. Model evaluation, *J. Geophys. Res.*, *111*(D6), D06302, doi:10.1029/2004JD005608.

Pun, B. K., R. T. F. Balmori, and C. Seigneur (2009), Modeling wintertime particulate matter formation in central California, *Atmos. Environ.*, *43*, 402–409, doi:10.1016/j.atmosenv.2008.08.040.

Raffuse, S. M., and L. R. Chinkin (2005), *Emission inventory reconciliation in the CRPAQS study area, Final Report, STI-902327–2751-FR, prepared for California Air Resources Board*, July, Sonoma Technology, Inc., Petaluma, Calif.

Tonse, S. R., N. J. Brown, R. A. Harley, and L. Jin (2008), A process-analysis based study of the ozone weekend effect, *Atmos. Environ.*, *33*, 7728–7736, doi:10.1016/j.atmosenv.2008.05.061.

Turkiewicz, K., K. Magliano, and T. Najita (2006), Comparison of two winter air quality episodes during the California Regional Particulate Air Quality Study, *J. Air Waste Manage. Assoc.*, *56*(4), 467–473.

Watson, J. G., D. DuBois, R. DeMandel, A. Kaduwela, K. Magliano, C. McDade, P. Mueller, A. Ranzieri, P. Roth, and S. Tanrikulu (1998), Aerometric Monitoring Program Plan for the California Regional $PM_{2.5}$/PM_{10} Air Quality Study, DRI Document No. 9801.1D5, Report prepared for California Air Resources Board, Sacramento, Calif.

Watson, J. G., and J. C. Chow (2002), A wintertime $PM_{2.5}$ episode at the Fresno, CA, supersite, *Atmos. Environ.*, *36*, 465–475, doi:10.1016/S1352-2310(01)00309-0.

Watson, J. G., J. C. Chow, D. H. Lowenthal, M. R. Stolzenburg, N. M. Kreisberg, and S. V. Hering (2002), Particle size relationships at the Fresno Supersite, *J. Air Waste Manage. Assoc.*, *52*, 822–827.

Wexler, A. S., F. W. Lurmann, and J. H. Seinfeld (1994), Modelling urban and regional aerosols: I. Model development, *Atmos. Environ.*, *28*, 531–546, doi:10.1016/1352-2310(94)90129-5.

Ying, Q., and M. J. Kleeman (2006), Source contributions to the regional distribution of secondary particulate matter in California, *Atmos. Environ.*, *40*, 736–752, doi:10.1016/j.atmosenv.2005.10.007.

Ying, Q., J. Lu, A. Kaduwela, and M. J. Kleeman (2008a), Modeling air quality during the California Regional Particulate Air Quality Study using the UCD/CIT source oriented air quality model: Part II. Regional source apportionment of primary airborne particulate matter, *Atmos. Environ.*, *42*, 8967–8978, doi:10.1016/j.atmosenv.2008.05.065.

Ying, Q., J. Lu, P. Allen, P. Livingstone, A. Kaduwela, and M. J. Kleeman (2008b), Modeling air quality during the California Regional Particulate Air Quality Study using the UCD/CIT source oriented air quality model: Part I. Base case model results, *Atmos. Environ.*, *42*, 8954–8966, doi:10.1016/j.atmosenv.2008.05.064.

Zhang, X. Q., P. H. McMurry, S. V. Hering, and G. S. Casuccio (1993), Mixing characteristics and water-content of submicron aerosols measured in Los-Angeles and at the Grand-Canyon, *Atmos. Environ, Part A-General Topics*, *27*(10), 1593–1607, doi:10.1016/0960-1686(93)90159-V.

Zhang, Y., B. Pun, K. Vijayaraghavan, S.-Y. Wu, C. Seigneur, S. Pandis, M. Jacobson, A. Nenes, and J. H. Seinfeld (2004), Development and application of the Model of Aerosol Dynamics, Reaction, Ionization and Dissolution (MADRID), *J. Geophys. Res.*, *109*(D1), D01202, doi:10.1029/2003JD003501.

M. Z. Jacobson, Department of Civil and Environmental Engineering, Yang and Yamazaki Environment and Energy Building, Room 397, Stanford University, Stanford, CA 94305, USA.

P. Liu, X.-H. Liu, and Y. Zhang, Department of Marine, Earth, and Atmospheric Sciences, 1125 Jordan Hall, Campus Box 8208, 2800 Faucette Dr., North Carolina State University, Raleigh, NC 27695, USA. (yang_zhang@ncsu.edu)

B. Pun and C. Seigneur, Atmospheric and Environmental Research, Inc., 2682 Bishop Dr., Suite 120, San Ramon, CA 94583, USA.

W.-X. Wang, Environment Research Institute, Shandong University, 27 Shanda Nanlu, Jinan City, Shandong Province, 250 100, China.